A STUDY OF PRECIPITATE MORPHOLOGIES IN Cu-Zn AND Cu-Zn-Sn ALLOYS

A STUDY OF PRECIPITATE MORPHOLOGIES IN Cu-Zn AND Cu-Zn-Sn ALLOYS

By

John Alexander Malcolm, B.Sc.

A Thesis

Submitted to the Faculty of Graduate Studies

in Partial Fulfilment of the Requirements

for the Degree

Master of Science

McMaster University

July 1966

MASTER OF SCIENCE
(Metallurgy)

McMASTER UNIVERSITY
Hamilton, Ontario

TITLE: A Study of Precipitate Morphologies in Cu-Zn and Cu-Zn-Sn Alloys.

AUTHOR: John Alexander Malcolm, B.Sc.

SUPERVISOR: Dr. G. R. Purdy

NUMBER OF PAGES: ix, 51

SCOPE AND CONTENTS:

The validity of current theories of precipitate morphology is dependent on the microscopic nature of the precipitate-matrix interface. It is the purpose of this thesis to investigate, by electron microscopy interfacial structure and mobility in precipitation reactions pertaining to these theories. In particular the $\beta \rightarrow \alpha$ Widmanstatten reaction in 60:40 brass is investigated and compared with the $\beta \rightarrow \gamma$ reaction in a Cu-Zn-Sn alloy.

ACKNOWLEDGEMENTS

The author would like to thank Dr. G. R. Purdy for suggesting the research problem and for his encouragement and help throughout all phases of the work. Gratitude is expressed to Dr. J. S. Kirkaldy for his assistance with the problem of interface stability. The author would also like to thank the technical staff of the Metallurgy Department for their help and in particular Mr. H. Walker for his assistance with the problems of electron microscopy.

The financial support of a McMaster Graduate Scholarship and an Ontario Graduate Fellowship is gratefully acknowledged.

TABLE OF CONTENTS

LIST OF TABLES

LIST OF ILLUSTRATIONS

INTRODUCTION

The role of phase transitions in metallurgical technology is obvious - however the metallurgist's ability to control and predict metallurgical structure is seriously limited because of a lack of detailed knowledge of transformation kinetics. Since many present day commercial alloys, requiring precise physical properties, are used in non-equilibrium conditions, this knowledge is being sought by an increasing number of workers. From a more academic point-of-view the study of phase transitions is attractive because of the precise macroscopic classification to which the field lends itself. Hence the statement of unifying principles appears feasible.

Several workers have proposed concepts of precipitate morphology control through phase boundary mobility. Detailed study of these interfaces has been limited in the past by the resolution of experimental techniques. The development of the electron microscope has provided researchers with a tool with which to test past speculation.

The aim of this investigation has been to study the structural and migrational characteristics of selected diffusional phase boundaries and to use this information to advance our understanding of the field. Most theories have centered on austenite proeuctoid ferrite boundaries, however this transformation is complicated by the martensite reaction above room temperature and the high diffusivity of carbon at high temperature.

The transformation of metastable β-brass has many aspects of the decomposition of austenite (eg. martensite, bainite, Widmanstatten α-β precipitation). The martensite in Cu-Zn forms at subzero temperatures for most compositions, thus it is possible to observe Widmanstatten interfaces by means of room temperature electron microscopy. In addition the $\beta \rightarrow \gamma$ transition in Cu-Zn-Sn alloys proved useful in demonstrating the effect of orientation on surface energy.

CHAPTER 1

Phase Transformation in Condensed Systems

1.1 Classification of Phase Transformations

A phase transformation is defined as a rearrangement of the structure (atomic, electronic) of an assembly. This rearrangement must eventually cause the appropriate thermodynamic potential (usually the Gibbs Free Energy) of the assembly to approach an optimum. The driving force for a phase transformation may be considered to be the difference in free energy of the initial and final configurations. The transformation path is strongly dependent on small fluctuations from the initial state of the system and particularly on whether these fluctuations raise or lower the free energy.

Phase transformations can be classified as to (a) solute redistribution (b) type of nucleation event and (c) interface type, Fig. 1.) This classification differs from the usual "experimental" classification[1] in that some of the definitions involved are based on indirect evidence rather than on macroscopic observables. In this brief review the author wishes to emphasize the role played by interfacial structure in phase transformations; this emphasis is facilitated by the classification given. Phase transformations are broadly classified as diffusional or diffusionless, although many diffusional reactions (e.g. the formation of Widmanstatten ferrite, bainite, $CuAu_{II}$) display characteristics usually associated with diffusionless (martensitic)

transformations. The present point-of-view is that a greater degree of understanding of the similarities between such disparate systems will be obtained by detailed examination of interface structures. This basis for synthesis has obviously been hindered in the past by limited resolution of the techniques employed to observe interfaces.

Before reviewing phase transformations the problem of nucleation will be discussed briefly. In considering nucleation, two different types of fluctuations must be recognized.[2] (a) considerable atomic rearrangement over small volumes and (b) very small rearrangement spread over large volumes. Transformations which can be divided into regions of product and parent phase at some intermediate stage in the reaction are termed nucleate and are characterized by fluctuations of type (a). Classical nucleation theory has shown that any such system is stable with respect to fluctuations on a small scale and that a critical nucleus size must be reached before the transformation proceeds. This constitutes the well known "free energy barrier".

Less common to alloy systems is the non-nucleate transformation. Here there is a spontaneous decrease in free energy, (i.e. no nucleation barrier) and the transformation takes place in all parts of the system simultaneously.

Solid state interfaces can be coherent, semicoherent or incoherent Fig. 2. The latter two types may be further classified into glissile or non-glissile boundaries. A non-glissile boundary requires thermal activation for its migration while a glissile boundary can move, more or less freely under the action of a suitable driving force (mechanical or chemical).

1.2 Diffusionless Phase Transformations

(a) Martensite Transformations: The martensite reaction is a type of displacive transformation. Buerger[3] defines a displacive transformation as a systematic distortion of the high temperature phase without changing the intrinsic bonding between atoms. The atomic movements in martensite formation are presumed to be similar to those in mechanical twinning. The martensite lattice may be produced from the parent by a homogenous deformation. This results in the well known surface relief effects associated with martensite formation.

There are two major phenomenological theories of the martensite transformation[4] (Bowles-Mackenzie, and Wechsler-Lieberman-Read). Their intrinsic assumptions are a lattice correspondence between phases and an interface plane of zero net distortion. This type of theory enables the habit plane, orientation relationship and shape change to be predicted, provided the lattice parameters and crystal structures of the two phases are precisely known.

Martensite appears generally in the form of lenticular plates which propagate by the motion of glissile, semicoherent interfaces. Both theory and experiment have shown that the plane of the martensite interface is irrational. Motion of glissile dislocation arrays or a fine scale twinning deformation[1] are two mechanisms by which the interface may migrate. Martensite reactions have been observed in many alloy systems (e.g. FeC[1], TiNi[6], CuZn) and although the detailed characteristics of the reaction vary markedly from system to system the properties discussed above appear to be quite general.

(b) The Massive Transformation: Massive transformations differ from martensites in that the reaction proceeds by means of a high energy incoherent interface so that there is, in general, no relation between lattices. The transformation is "reconstructive"[3] i.e. a new lattice must be generated from the boundary. This reaction is usually found in eutectoid systems although it was first discovered in Cu-Zn alloys[6]. The massive phase is a supersaturated extension of the equilibrium low temperature phase. Morphologies are usually block like with distinct crystallographic facets (this feature will be discussed in detail later). Shapiro[7] has recently shown that the mobilities of both massive interfaces and incoherent grain boundaries are large and of the same order of magnitude.

(c) Second Order Diffusionless Transformations: The thermodynamic classification of phase transitions is based on the order of the lowest derivative of G (Gibbs Free Energy), with respect to temperature which exhibits a discontinuity. In first order transitions there are discontinuities in the first derivatives of G with respect to temperature and pressure (i.e.) entropy and volume). In a second order transition the entropy and volume are continuous and the second derivatives (eg. specific heat and compressibility) are discontinuous.

Christian[1] notes that the free energy of product and parent phases in a second order transition must lie on the same curve and thus they cannot co-exist in equilibrium. This implies that it is impossible to produce a metastable, undercooled parent phase. The above thermodynamic description also implies the existence of diffuse interfaces.

Barium Titanate ($BaTiO_3$)[3] undergoes a cubic to tetragonal second order transition involving a continuous series of crystal structures. Dautovich and Purdy[5] have recently reported the existence of a second order transition on cooling TiNi, "involving a sequence of cumulative lattice perturbations". Electron microscopic observation failed to resolve distinct interfaces.

1.3 A. Diffusional Transformations

(i) Nucleation and Growth Transformation: These transformations are characterized by the formation of a "classical" nucleus and subsequent growth in alloys via solute redistribution. Growth is thermally activated and usually diffusion controlled. Three types can be distinguished (1) General (2) Cellular (3) Guinier-Preston zone formation.

General precipitation is simply growth of isolated precipitates from supersaturated solid solution. Cellular precipitation involves the co-operative formation of two product phases. The following reactions may occur:

$$\alpha \rightarrow \text{depleted } \alpha + \beta$$

$$\alpha \rightarrow \beta + \gamma$$

For a complete review of cellular precipitation the reader is referred to the work of Shapiro[7]. Guinier-Preston zone formation involves the coalescence of atoms of solute into coherentclusters, a process which may be associated with a metastable spinodal system (see below). Age hardening systems are often characterized by several intermediate stages

between the initial formation of coherent Guinier-Preston zones, and the final incoherent precipitation of equilibrium phases[9].

(ii) Spinodal Transformations: Second order diffusional phase changes are termed spinodal reactions. There is a continuous fall in free energy and hence no need of a classical nucleation event. This reaction is commonly supposed to take place in systems which exhibit an equilibrium miscibility gap, the high temperature phase spontaneously decomposing into phases of identical crystal structure but varying concentrations of solute (eg. Cu-Ni-Fe).

Inside the spinodal curve (defined as the locus of points where $\frac{\partial^2 G}{\partial c^2} = 0$) $\frac{\partial^2 G}{\partial c^2}$ is negative and hence the diffusion coefficient is negative. If elastic constraints are overcome by sufficient undercooling, random concentration differences will be self enhancing by means of uphill diffusion and a modulated structure will result. Initial stages of of spinodal decomposition will therefore involve the formation of diffuse interfaces[9].

(iii) Order Disorder Transformations: Most order disorder transitions are first order reactions (eg. Cu_3Au, CuAu). β-Brass, however, appears to exhibit a second order transition, as is predicted from theoretical considerations of ordering reactions in b.c.c. AB compounds. For a complete review of order-disorder reactions see reference (8).

1.3 B Diffusional Transformations Exhibiting Similarities to Shear Reactions

Bainite is the name given to the transformation product of austenite at temperatures above that of martensite and below that of fine pearlite.

Bainite, Widmanstatten ferrite and Widmanstatten cementite show surface relief effects and grow isothermally. They may be thought of as transformations sharing characteristics of both nucleation and growth and martensite reactions.

The bainite transformation can be divided into two parts, upper and lower bainite, with a transition temperature of about 350°C in many steels. In lower bainite the carbide is contained within elongated ferrite plates in the form of small, plate shaped, particles oriented at about 60° to the axis of the plate. The ferrite edge has a sharp radius of curvature and is free of carbide while the sides of the plate have carbide particles in contact with the interface. There is some evidence that, along with carbide precipitation, there is some partition of carbon between the austenite and ferrite during growth[11]. In the upper bainite region the cementite plates appear to form from the parent austenite and are oriented roughly parallel to the ferrite plate axis. There is a distinct carbon enrichment of the austenite and upper bainite appears to grow initially as carbon saturated ferrite.

Ko and Cottrell[12] pointed out that due to the observed shape change, the thickening mechanism of bainite plates should be related to martensite growth. Speich[13] confirmed the shape change as due to an invariant plane strain. With regard to lower bainite, the interface is assumed to be martensitic but growth can only take place if there is carbide precipitation in the ferrite so as to increase the driving force. Thus lower bainite can be considered as martensite with an insufficient driving force for growth.

Hillert[4] notes the continuity of structure between isolated Widmanstatten ferrite and cementite, and upper bainite. It may be postulated that the growth of low carbon ferrite in upper bainite is martensitic in the sense that the interface is semicoherent and glissile but that the rate is controlled by the rejection of carbon into the austenite rather than precipitation from within. The glissile interface would account for rapid growth at temperatures where iron atoms are not able to diffuse fast enough to destroy the lattice correspondence. A consequence of this reasoning is that bainite type transformations should only be possible in alloys where the solute occupies interstitial sites[1].

Contrary to this conclusion, "bainite" reactions have been reported in a limited number of substitutional alloys where diffusion rates of solute and solvent are comparable (i.e. Cu-Zn, Cu-Al). It has been suggested that, in these alloys, the transformation may involve no composition change i.e. that the reaction is simply a high temperature isothermal martensite[1].

1.4 Application of Martensite Phenomenological Theory to Nucleation and Growth Transformations.

In view of the above discussion it seems plausible that martensite crystallography can be applied to bainite type reactions. Otte and Massalski[15] have successfully applied the Wechsler-Liebermon-Read theory to several diffusional reactions. (Widmanstatten α from β brass, Fe_4N and Fe_3P from α iron) For the cases of fcc $\rightleftharpoons$ bcc, fcc $\rightleftharpoons$ bct, bcc $\rightleftharpoons$ fct transformations, the indices of the invariant plane are given as:

$$h = \frac{1}{2n_1}\sqrt{\frac{n_1^2 + n_2^2 - 2n_1^2 n_2^2}{1 - n_2^2}} - \sqrt{\frac{2 - n_1^2 - n_2^2}{1 - n_2^2}}$$

$$k = \frac{1}{2n_1}\sqrt{\frac{n_1^2 + n_2^2 - 2n_1^2 n_2^2}{1 - n_2^2}} + \sqrt{\frac{2 - n_1^2 - n_2^2}{1 - n_2^2}}$$

$$l = \frac{1}{n_1}\sqrt{\frac{n_1^2 - 1}{1 - n_2^2}}$$

For the bcc $\rightleftharpoons$ fcc transformation $n_1 = \frac{a^\circ_{fcc}}{a^\circ_{bcc}}\,2$ and $n_2 = \frac{a^\circ_{fcc}}{a^\circ_{bcc}}$. The relative volume of product phase with respect to the parent phase is given by $n_1^2 n_2$. The variation of habit plane with relative volume is illustrated in Fig. 3.

CHAPTER 2

Interface Structure and Mobility

Introduction:

Because of the similarity between interphase boundaries and grain boundaries a brief description of the dislocation structure and energy of the latter will first be presented. The reader is referred to reference (16) for a more complete review of the subject.

2.1 Dislocation Models of Grain Boundaries

A grain boundary constitutes the transition zone between two crystals in contact, but differing in spatial orientation. Five degrees of freedom must be specified to describe the grain boundary interface crystallography. Three of these specify the relative orientations of the two crystals, while the remaining two specify the orientation of the interface plane.

When the orientation difference between two grains is small, the boundary can be described as an array of dislocations. In the simplest case[17] the crystals are connected by a rotation about an axis in the boundary and can be described by a row of dislocations with Burgers vectors normal to the contact plane. If the axis of rotation is not in the plane of the boundary, two types of dislocations with mutually perpendicular Burgers vectors must be introduced. An array of screw dislocations will describe a boundary with rotation axis perpendicular to the contact plane.

The interface in a large angle grain boundary is usually considered as a two dimensional disordered array with no correlation between the lattices of the two crystals. An alternative theory proposed by Mott[18] is that the boundary structure consists of regions of good and poor atomic matching. This point will be reconsidered later in the light of present experimental findings. A special type of high angle boundary is the "coincidence site" boundary[1]. These result from two grains rotated by fixed amounts with respect to each other about a common axis which is normal to a close packed plane. An appreciable fraction of atomic sites in these boundaries are common to both crystals. This will probably result in a lowering of the energy and mobility. The correspondence lattice concept, however, has little value in the description of two phase systems.

Read and Shockley[19] and Van der Merwe [20] have calculated grain boundary energies, as a function of misorientation angle, from elasticity theory. The general result is that grain boundary energies increase with increasing misorientation with small experimentally undetectable cusps at rational angles ($\theta = \frac{1}{m}$) and large cusps at twin orientations.

2.2 Interphase Boundaries

Interphase boundaries are similar, in many ways, to grain boundaries. Again five degrees of freedom are needed to specify the boundary crystallographically. However, it is not possible to bring the two lattices into coincidence by means of a simple rotation.

2.3 Incoherent Interphase Boundaries

There is no correspondence between lattices across an incoherent interphase boundary. Smith[21] describes them as essentially two dimensional liquid layers, similar to high energy grain boundaries. Diffusion can take place along or across the interface, thus it is mobile at elevated temperatures. Aaronson[22] notes that if all the orientations a precipitate may have with the matrix are considered, most will have poor atomic matching (i.e. are incoherent). If an equilibrium structure can be assumed in these boundaries atoms will oscillate between compromise positions in the two lattices.

On the subject of mobility, Aaronson states that incoherent boundaries like high angle grain boundaries migrate by means of unrestricted movement of atoms across the boundary. This is verified by the calculation of Shapiro[7]. The rate controlling factor in migration is the long range diffusion of solute away from or toward the boundary (except in massive reactions, where mobility must be rate-limiting).

Grain boundary precipitation of ferrite from austenite at low undercooling (so-called allotriomorphs[22]) are assumed, in general, to have at least one incoherent interface[21] and, under these conditions growth will proceed by the motion of this interface. Also, the tips and sides of side plates and intergranular Widmanstatten plates with low radii of curvature should be disordered. Growth kinetic experiments on these morphologies are generally in fair agreement with diffusion control theory[23].

2.4 Coherent Interphase Boundaries

The process of mechanical twinning provides the simplest example of a coherent boundary. All vectors in the composition plane are unchanged by shear, and the two lattices match exactly at the interface. In general, it is not possible to find a plane of exact matching between two different crystal structures. Here, long range coherency is possible only if the unit cells of the crystals have a zero value of one principle strain. This requirement is fulfilled in a few cases: for example, the fcc $\rightleftharpoons$ hcp transition where the octahedral and basal planes have nearly identical interatomic distances[22]. In cases where the misfit is small the two lattices may be forced into coherency with the surrounding area, accommodating the elastic strain. This condition can be satisfied only if the interface area is very small and is observed, for example, in precipitation involving Guinier-Preston zones.

Smith[21] pointed out that it is possible for coherent boundaries to migrate but that accumulated volume strain soon forces them to stop. As a coherent boundary migrates there will be a macroscopic change of shape due to the correspondence between lattices.

2.5 Semicoherent (Dislocation) Interfaces

The theory of martensite transformations is based on the postulate that the habit plane is an invariant plane (zero net distortion) of the macroscopic shape deformation. In general the structures at the interface do not match perfectly, but the mismatch is periodically corrected by

dislocations or twin boundaries. This is an example of a semicoherent interphase boundary which consists of regions where the two structures are forced into elastic coherence separated by regions of misfit, and is considered analogous to a low angle grain boundary. Since there is localized coherency the migration of a semicoherent interface will produce a shape change which is an invariant plane strain.

Christian[1] discusses two idealized models of semi-coherent boundaries. The first contains a single set of parallel dislocations with common Burgers vectors not lying in the interface. It is possible then, that the glide planes of the dislocations meet end to end at the interface. The lattice invariant deformation produced by the dislocations is a simple shear, as is believed to exist at martensite interfaces. The migration of this boundary is conservative (i.e. the number of lattice points in a given volume of parent and product phases is the same) and glissile.

The second type contains parallel dislocations with common Burgers vectors in the interface plane and not parallel to the dislocation lines. The habit plane is now the glide plane and the dislocations are sessile with respect to migration of the boundary normal to itself. Normal migration can only take place by synchronous climb of the dislocations. If this model is extended to three dimensions the boundary becomes a cross grid of dislocations. Van der Merwe [20] has calculated the energy for this "epitaxial" type interface and found it comparable to low angle grain boundaries.

2.6 Interfacial Energy

Interphase boundaries are characterized by disregistery. This is defined as:

$$\delta = \frac{(a_\alpha^\circ - a_\beta^\circ)}{a_\alpha^\circ} \qquad (2.1)$$

where a_α° and a_β° are the lattice parameters of the phases α and β in the absence of distorting forces.

The energy of an interface is believed to consist of two parts[25]:

1) Chemical interfacial energy σ_c - this is the localized elastic energy due to bonding across a coherent interface.
2) Structural interfacial energy σ_{st} associated with any lack of coherency between the two structures.

For small values of disregistery the chemical and structural terms are approximately additive. i.e.

$$\sigma \sim \sigma_c + \sigma_{st} \qquad (2.2)$$

If the lattices of the two adjoining phases are strained by an amount e at the interface the disregistry is reduced to:

$$\delta' = \delta - e \qquad (2.3)$$

On the basis of a dislocation model of a semicoherent interface Brooks[26] derived the energy as:

$$\sigma_{st} = L\delta' [M - \ln \delta'] \qquad (2.4)$$

where L and M are evaluated from the elastic constants of the two structures and the boundary entropy is assumed negligible.

Interphase boundary energies corresponding to small disregistery have not been determined but the results of Smith[27] show that σ for incoherent α-β boundaries have a lower value than for grain boundaries in either the α or β phases. Smith[28] has questioned the validity of equilibrium energy measurement applied to kinetic systems since a moving boundary will presumably acquire a higher amount of imperfections.

2.7 Theory of Interface Motion

Two major mechanisms of crystal growth may be distinguished[29]; (1). The interface advances by the lateral motion of steps, a multiple of one interplanar distance in height. The steps are considered as transition areas between two regions of surface parallel to each other separated only by the step. By this definition, both sharp and diffuse interfaces can contain steps, the step height in the diffuse interface being smaller than the thickness of the interface.

(2). The surface advances normal to itself without the use of steps. This means that in the presence of a suitable driving force, each element of the surface is capable of continued change.

In order to determine which mechanism will be operative in a given system two criteria are generally used.

(1) Is the interface diffuse? A diffuse interface is characterized by a gradual change (several interplanar distances) between phases, whereas in a sharp interface the phase change is accomplished over one interplanar distance. The diffuse interface is thought to be able to advance normal to itself.

(2) Is the interface singular? A singular interface is one for which the interfacial energy as a function of orientation has a pointed minimum. Singular interfaces must advance by the ledge mechanism whereas, it is believed non-singular interfaces can advance normal to themselves.

Another criterion, proposed by Cahn[30] is the ability of an interface to reach equilibrium in the presence of a driving force. The lateral growth mechanism will be found when an interface can reach a metastable equilibrium configuration. It will tend to remain in this configuration and can do so only by the passage of steps.

Cahn concludes that for all types of interface the mechanism of interface migration depends on the magnitude of the driving force rather than the nature of the interface. At sufficiently high driving forces an interface can move uniformly without the benefit of ledges although for sharp interfaces the magnitude of the driving force required may be so high that it may never be achieved in practice.

Interfacial free energy can be divided into two terms. The first due to surface tension and the second due to lattice resistance to interface motion. As an interface which has acquired metastable equilibrium, moves through the lattice it must pass through higher energy states in getting from one equilibrium position to the next. This periodic restraining force tends to keep a sharp interface parallel to low index planes.

As a singular interface is displaced from its equilibrium configuration its energy and step density will increase with increasing angle of deviation[31]. For example, if two crystallographically equivalent directions which define the equilibrium configuration are 90° apart, the plot of interfacial free energy vs. angle of rotation about an axis in the boundary will

have the form shown in Fig. 4 (a). Steps, in this case, will resolve the boundary into a series of crystallographically equivalent singular interfaces while macroscopically the boundary will appear as a high energy type. The energy of a stepped boundary can increase only to the value of an incoherent boundary in the same system, i.e. E_1 or E_2 in Fig. 4.(a).

2.8 Precipitate Morphology Control

(a) Structural Consideration: Aaronson[22] notes that the simplest semicoherent interphase boundary is found in the fcc$\rightleftharpoons$hcp transition described by the relation $(111)_{fcc} \parallel (0001)_{hcp}$ $[110]_{fcc} \parallel [11\bar{2}0]_{hcp}$ (Fig. 5a). Partial coherency can be achieved by periodically introducing an edge dislocation in the closely matching rows with Burgers vector parallel to the row. In the case of the fcc$\rightleftharpoons$bcc reaction the situation is more complex (Fig. 5b). The Kurdjumov Sachs orientation relationship[32] $(111)_{fcc} \parallel (110)_{bcc}$ $[110]_{fcc} \parallel [111]_{bcc}$ provide close matching along only one close packed direction. Brooks[26] feels that the misfit dislocation spacing in this interface would be so small that it will reduce to an incoherent one while Paxton[33] objects on the grounds that the elastic energy for even partial coherency is much too high. It is concluded that the structure approximates arrays of closely spaced dislocations bounding areas of total incoherency.

(b) Aaronson's Theory: The factors which control the morphology of proeutectoid ferrite has been the subject of several theories[22]. No theory, however, gives a complete description. Aaronson ascribes the formation

of geometrical precipitates to interface mobility control. Dislocation interfaces are formed at one, or a few orientations of the precipitate with respect to the matrix, while the remaining interfaces will be incoherent and thus their growth will be controlled by long range diffusion. Since the total amount of semicoherent boundary area increases with time at transformation temperature[21], these orientations probably correspond to energy cusps. If the migration of the semicoherent boundary proceeds by the thermally activated climb of dislocations, the growth rate should be near zero and undetectable However, these interfaces have a small, but readily detectable migration rate.

Assuming that these boundaries contain sessile dislocations Aaronson proposes that thickening proceeds via the formation and lateral growth of ledges. This would enable the interface to appear macroscopically curved but in reality maintain a strict habit plane. The steps normal to the boundary have a disordered structure and would be able to migrate rapidly. The overall rate of migration of the boundary would be controlled by the height, density and rate of lateral movement of the ledges. This rate is clearly less than that permitted by volume diffusion control.

Recently this theory has been verified for the $\delta_{fcc} \rightleftharpoons \gamma_{hcp}$ transition in Al-Ag alloys. Hren and Thomas[34] reported that the thickening of coherent γ' plates, in an Al-20% Ag alloy, proceeds entirely by the formation and lateral movement of ledges. Aaronson and Laird [35] have investigated the dislocation structure of the broad faces of γ plates in an Al-15% Ag alloy. They found the interfaces to be comprised of three different arrays of dislocations. In all the arrays the dislocations were

sessile with respect to boundary migration and of the $\frac{a}{6}$ [112] partial variety. Since these observations have been made on an interface where there is extremely good atomic matching it is doubtful whether this evidence can lend support to a general theory of precipitate morphology.

(c) Shewmon's Hypothesis: If interfacial equilibrium is maintained between a growing precipitate and a supersaturated matrix, so that solute diffusion alone determines the growth rate a "dendritic" morphology should be observed. This effect, which is commonly observed in the solidification of molten metals and alloys is largely absent in precipitation from supersaturated solid solution.

For a planar interface under local equilibrium conditions, any perturbation will tend to grow out ahead of the planar segment due to the higher gradient ahead of it[36]. Thus a planar interface is unstable with respect to an irregular one. Mullins and Sekerka[37] have investigated the stability of a sinusoidal perturbation in shape imposed on a moving planar interface between a stable and a supersaturated phase. They found that surface tension provides the main stabilizing force for a case where interfacial equilibrium exists. This stabilizing force will be completely overcome if the radius of curvature of the perturbations is of the order of 1μ or greater or if the supersaturation is greater than about 10%.

Because of the lack of instability in solid-solid interfaces, Shewmon[38] attributes the observed growth rate of geometrical proeutectoid ferrite precipitates to a slow interface controlled reaction at all precipitate matrix orientations with the exception of an interface propagating roughly

parallel to the $(111)_\gamma$ for the case of the Kurdjumov-Sachs orientation relation. He applied this model to high temperature precipitation of proeutectoid ferrite to explain the rare occurence of Widmanstatten side plates.

CHAPTER 3

The Copper-Zinc System

Introduction:

The properties of Copper-Zinc alloys, especially those containing high copper, have been extensively studied. The strength, ductility, machinability and corrosion resistance of alpha brass make it one of the most useful non-ferrous metals. β-brass, however, is too brittle at room temperature to be of much commercial use. Pertinant data on the copper-zinc system is given in Table 1 and Fig. 6-9.

3.1 Elastic Anisotropy of β-Brass

The stability criteria require, for a given crystal, that each of the principal minors of the determinant of the elastic coefficients be positive[39]. For cubic systems the conditions are:

$$C_{11} > 0 \tag{3.1}$$

$$C_{44} > 0 \tag{3.2}$$

$$C_{11}^2 > C_{12}^2 \tag{3.3}$$

$$C_{11} + 2C_{12} > 0 \tag{3.4}$$

For β-Brass, the value of the third condition $(C_{11}^2 - C_{12}^2)$ is 0.445 compared with 3.628 for α-iron, which indicates this system is on the verge of instability. This property is shared by many β-phase alloys and

is exemplified in their high elastic anisotropy For β-brass the ratio of the two shear coefficients ($2C_{44}/C_{11}-C_{12}$ = 18) indicates a low resistance to shear along the face diagonal i.e. (110) [110]. This phenomenon has been attributed to a negative contribution to the elastic shear constant from the closed ion shells plus a positive contribution from the electrostatic reaction[40]. The foregoing has also been used to explain the positive temperature coefficient of $E_{(110)}$ and $E_{(100)}$ below 200°C[40].

3.2 The Decomposition of Metastable β-Brass

(i) The martensite transformation: A martensite transformation is observed in 60:40 brass when the metastable β-phase is cooled below room temperature[41-47]. The proposed face centered tetragonal[44] and coexisting monoclinic and triclinic[45] unit cells have not been in good agreement with X-ray data. Recently Jolley and Hull[47], using electron microscopy and diffraction, concluded that the martensite has an orthorhombic structure with a = 2.670 Å, b = 4.270 Å, c = 4.460 Å. Their results agree quite well with W-L-R theory.

The transformation starts with the appearance of thin lamallae parallel to the $\{2,11,12\}_\beta$ planes[42]. The bands merge with each other to form a final zig-zag structure. The shape deformation has been analysed as a shear, parallel to the habit plane, in a direction close to $[011]_\beta$[44]. The bands contain a high density of striations with a spacing of approximately 25 Å which are believed to be either twins or stacking faults. M_s temperatures vary from 20°C at 61.46% Cu to -131°C at 59.96% Cu[48].

The martensite transformation has also been induced by room temperature deformation[41,49]. The M_D temperature, corresponding to the appearance of strain induced martensite is about 300°C higher than that observed without strain. Massalski and Barrett[49] found that alloys containing as much as 51.89% Zn could be transformed into a faulted hcp structure by cold working at liquid nitrogen temperatures. This transformation has been postulated as the cause of the initiation of fatigue cracks in β-Brass at low temperatures[50].

Hull[51] has observed that foils of β-brass containing 61% Cu transform spontaneously, upon thinning, to an fct structure. The product is highly twinned, like the martensite, but no specific habit plane is observed. A shear mechanism is proposed, and because surrounding restraints are removed in the thin foil, the reaction can take place spontaneously.

(ii) The Massive Transformation: Hull and Garwood[42] found that, on cooling a 61.3% Cu specimen rapidly enough to room temperature, the metastable β' phase was completely retained. Massive α is formed by a slower cooling rate. Massive crystals form as blocks with distinct crystallographic facets. The habit planes of the facets are the same as those of the subzero martensite $\{155\}_\beta$ - $\{166\}_\beta$. The critical composition range for the formation of massive α is 68.5 - 59% Cu.[52].

(iii) The Widmanstatten Reaction: Widmanstatten morphologies can be obtained in a 60% Cu brass either by cooling in air from the β phase field or by quenching and tempering at temperatures greater than ∿ 450°C for very short times. Orientation relationships are of the Kurdjumov-Sachs type while the interface plane of the Widmanstatten is the same as that of

the subzero martensite[15].

(iv) The Bainite Reaction: The isothermal decomposition product of metastable β-brass, below 350°C, is termed bainite. Garwood[53] has reported that this "bainite" reaction, in a 58.7% Cu alloy, shows surface relief effects and the same habit planes as the subzero martensite. It is hypothesized that, like the iron carbon bainite reaction, coherent isothermal growth is possible only if solute (zinc) is rejected into the matrix.

Shinoda and Amano[54], using divergent-beam X-ray back reflection techniques, have determined that the β→α bainite transformation involves a series of bct and fct intermediate structures with varying axial ratios. Bassi and Strom have concluded, from X-ray data, that a 60% Cu brass, tempered at 150°C yields a body centered monoclinic precipitate.

3.3 Orientation Relationships

The orientation relationships between α-β and β-α phases have been investigated by means of solid vapor diffusion couples[55]. Alpha phase formed on beta phase took orientations clustering about the Kurdjumov-Sachs ($(110)_{bcc} \parallel (111)_{fcc}$ $[111]_{bcc} \parallel [110]_{fcc}$) and Nishiyama ($(110)_{bcc} \parallel (111)_{fcc}$ $[110]_{bcc} \parallel [211]_{fcc}$) relationships. Beta phase formed on gamma phase and gamma formed on beta took orientations with cube axes in both phases parallel. Measurements made by Hu and Smith[56] on recrystallized α-β brass confirm the K-S relationships. They estimate that the surface energy of α-β boundaries is roughly 20% less than that of α-α (or β-β) boundaries.

3.4 Equilibrium Relations

Examination of the free energy vs. composition diagrams of α, β and γ brass[57] (Figs. 7 and 8) indicates that a eutectoid transformation ($\beta' \rightarrow \alpha + \gamma$) is possible. Shinoda and Amano[58] have investigated this possibility and have proposed a eutectoid transformation of β' at 52.5% Cu at approximately 250°C as shown in Fig. 6b.

These results were obtained by annealing samples below 250°C for times in the order of months. X-ray diffractometric and metallographic results showed evidence of α and γ phases although the amounts present were not consistent with the present positions of the $\alpha/\alpha+\beta'$ and $\beta'/\gamma+\beta'$ phase boundaries.

CHAPTER 4

Experimental

4.1 Single Crystal Experiments

Preliminary experiments on α-β brass phase boundary migration were carried out by means of solid-vapor diffusion couples, using single crystal copper spheres. The spheres were grown in a vertical tube furnace by the Bridg man technique with a mold lowering speed of 3.1 inches per hour. A split graphite mold was employed with a half sphere drilled in each side, and a hydrostatic head maintained above the spherical cavity Fig. 10. For lowering purposes the mold was enclosed in a tight fitting graphite sheath. A charge of copper rod (99.995%) was introduced into the hydrostatic head and the mold lowered through the furnace. Two passes through the hot zone were made, the first to melt the copper and allow it to run into the spherical cavity and the second to insure the growth of a single crystal. The sphere was then chemically polished, using a solution containing 50 ml HAc, 10 ml H_2PO_4, 10ml HCl and 30 ml HNO_3 at a temperature of 70°C. The chemical polish was found to produce a surface, comparable in quality to an electropolished one. Examination of the chemically polished crystals by Laue back reflection indicated a single crystal with very little distortion.

The crystal was then placed in a vycor tube with a quantity of brass turnings (50% Zn) separated from the crystal by glass wool. The

tube was flushed several times with argon and sealed off under a partial pressure (100 mm Hg) of hydrogen. The reaction was carried out in a muffle furnace. Optimum conditions were determined to be 500°C for 1 hr. A longer time at temperature produced a retrograde movement of the α-β boundary due to depletion of the zinc source, or recrystallization of the α substrate, while a shorter time did not produce a sufficiently thick layer for observational purposes.

After the reaction the tube was immersed in ice water and shattered. The crystal was then examined by the Laue X-ray method. In order to examine the crystal metallographically it was necessary to prevent any rounding of the edges. Coating the crystal with epoxy resin before mounting in bakelite was found to be the best method of edge preservation.

4.2 Preparation of Alloys

Brass alloys of 60.4 wt % Cu and 54.5 wt % Cu were prepared using zone refined zinc (99.999%) and electrolytic copper (99.99%). Induction melting was used with the materials in a graphite crucible and under a borax slag. The mixture was allowed to remain molten for 5-10 seconds; then just after solidification, the crucible was quenched into ice water. In a preliminary melt a bronze alloy of composition 56.5 wt % Cu, 39.5 wt % Zn 4.0 wt % Sn was made and subsequently used in the investigations. Spectrographic analysis of all alloys used revealed negligible amounts of impurities (Table 2).

The alloy ingots were sectioned and hot rolled at 650°C to sheet 0.03" thick. The sheets were homogenized in air at 800°C for 1 min. and

rapidly quenched into ice cold brine to retain the metastable β-phase A portion of the 60.4% alloy was given a less drastic quench in order to obtain a Widmanstatten structure on cooling. In order to prevent the metastable β phase from aging appreciably all alloys were kept at 0°C prior to heat treating.

4.3 Heat Treatment

The alloy sheets were cut to dimensions of 1" x 1/2" to facilitate the heat treating procedure. The tempering heat treatments were carried out in a salt pot containing a low melting point $NaNO_2$, KNO_3 mixture. Temperature control was $\pm$ 5C°. After heat treatment the samples were further thinned to 0.008" by chemical polishing in order to minimize the electropolishing time.

4.4 Light Microscopy

Optical microscopy was carried out on quenched and tempered specimens to determine the probability of isolating precipitate in a thin foil. The etchant used was a 10% aqueous solution of copper ammonium chloride neutralized with NH_4OH. This solution darkens β-brass.

4.5 Electron Microscopy

(i) Preparation of thin foils: The electropolishing method was essentially the same as reported by Kay[59] for polishing single phase β-brass alloys. The "window technique" was used with an electrolyte of nitric

acid (1 part) in methanol (2 parts). The cell potential was 6-8 volts and the electrolyte temperature was kept close to -20°C. The specimen was held by an alligator clip and both the clip and the perimeter of the specimen were coated with Microstop lacquer. Throughout the polishing operation the specimen was gently agitated to remove a black anodic deposit. It was found that one application of the microstop was sufficient since holes appeared, more or less, randomly on the specimen surface. As soon as a suitable area had formed the sample was withdrawn from the electrolyte with the voltage still on, rinsed in methanol, cooled with dry ice and placed in cooled methanol in a shallow dish. For sectioning purposes, the foil was removed from the methanol and placed between two pieces of watchmakers tissue, then cut with a surgical blade. The specimen was immediately inserted into the microscope specimen holder using 75 mesh grids.

(ii) Microscope Operation: The microscope used was a Siemens Elmiskop I operated at 100KV using projector pole piece III[60]. Magnification calibration was accomplished by a series of photographs of a carbon replica of a diffraction grating while rotation calibration was done using MoO_3 crystals.

(iii) Trace analysis: Trace analysis were carried out on boundaries for which sufficient diffraction could be obtained. This method, however, contains several sources of error.[61]

1) Errors in the determination of the crystallographic orientation of the specimen.
2) Errors in the calibration of the image rotation due to a change in intermediate lens current.

3) Uncertainty in the specimen thickness.

4) Inaccuracy in the plotting and manipulating of stereograms.

Specimen thickness, determined by measuring boundary extinction fringes, proved to be the largest source of error.

CHAPTER 5

Experimental Results

Introduction:

Although the main topic of this thesis is the observation and comparison of interphase boundaries in the Cu-Zn and Cu-Zn-Sn systems, two essentially unrelated topics will be discussed although no definite conclusions about them have been made. These include observations on internal structure in the massive α phase (Sec. 5.2) and observations on high zinc β-brass alloys (Sec. 5.3). The main topics will be presented in sections 4 and 5 with preliminary experiments reported in Section 1.

5.1 Single Crystal Experiments

Recrystallization of the α brass layer during the reaction prevented a precise crystallographic analysis by Laue back reflection. Several crystals were sectioned in such a way that a $\{111\}_\alpha$ plane was included in the plane of polish. In all cases the thickness of the β-brass layer was constant for all orientations including the $\{111\}_\alpha$ and was ∿2μ thick. In areas where severe recrystallization took place the α brass region was observed to have grown more rapidly by means of grain boundary diffusion.

5.2 Observations on the Massive α Phase

The as quenched massive α phase showed a large density of stacking faults and dislocations, (Fig. 11).

On tempering the massive specimens for 3 hrs. at 200°C a subgrain structure was revealed. Fig. 12(a) shows such a sub-boundary in which the planar segments make an angle of ∿72° with each other. The misorientation between the two grains was so small that it was impossible to determine from selected area diffraction. The boundaries in Fig. 12(b) are composed of planar segments. The misorientation between each grain is 7°.

5.3 Precipitation in 54.5% Cu Brass

As quenched foils of this composition were observed to develop a structure while in the microscope. The resulting structure is shown in Fig. 13 and is similar to that observed in the early stages of spinodal decomposition. This contrast was very orientation dependent for a slight tilt would make it disappear.

After tempering for 24 hrs. at 200°C structures similar to Fig. 14(a,b) were observed. Precipitate displacement fringe contrast can be seen in Fig. 14(b). Both micrographs indicate that the precipitate develops in distinct crystallographic directions.

Selected area diffraction of the quenched foils showed continuous streaking in <112> . In the tempered alloy distinct maxima occurred on these streaks while the general streaking became less obvious (Fig. 14(c)).

5.4 Precipitation in the Cu-Zn-Sn Alloy

(a) Intergranular precipitates: The morphologies of intergranular precipitates formed by tempering for different times are shown in Figs. 15, 16, 17. These "dendritic" precipitates were dispersed evenly throughout the alloy when observed using optical metallography. In each case, at least one of the main growth directions of the dendrite was parallel to $\langle 110 \rangle_\beta$. The branches from these main directions were also, in general, parallel to $\langle 110 \rangle_\beta$.

X-ray diffractometry verified that this precipitate was similar to γ-brass, although exact lattice parameter measurements were not made. Most selected area diffraction patterns were similar to that shown in Fig. 18. Many precipitate spots are coincident with matrix spots and the unit cell of the precipitate triples along the $\langle 110 \rangle_\beta$.

Misfit dislocations were observed in the secondary branches of most dendrites. As shown in Figs. 16 and 17 the misfit dislocation spacing is quite large, indicating reasonably good fit between precipitate and matrix.

(b) Grain Boundary Precipitation: Precipitate nucleated at grain boundaries was observed to grow into one grain only. At short times (Fig. 19) the precipitate assumed a bumpy interface which could be approximated to sinusoidal perturbations with a wave length of 400 Å. Fig. 19(b) shows several of these perturbations which have grown out ahead of the general interface. At longer times secondary arms were observed to grow out of the main ones as in the intergranular precipitate.

Selected area diffraction of Fig. 19(a) indicated that the precipitate grew into the grain with which it had partial lattice matching (as in Fig. 18).

5.5 Widmanstatten Precipitation

(a) Precipitate formed on continuous cooling: A previous investigation of the $\beta \rightarrow \alpha$ Widmanstatten reaction in brass concluded that on continuous cooling needles are formed instead of plates[62]. The microstructure in Fig. 20 gives a fair indication of the needle like morphology. A calculation of the growth rate of this particular composition as a function of diffusion coefficient and phase boundary composition was made using the Zener method [63] (Fig. 22). Foils made of the as quenched material were badly etched and only a limited amount of information could be obtained. The α-β boundaries appeared to be smooth, but a complete verification of this was impossible.

After a tempering heat treatment of 1 hr. at 200°C the foils produced were of a much better quality. Both phases seemed to etch at approximately the same rate. Most interfaces observed in this condition contained facets plus a rather complicated dislocation structure both in the boundary and behind the boundary in the α phase (Figs. 21, 23, 24,25). Precipitation occurred in both the α and β phases as a result of the tempering heat treatment. No distinct morphology was observed in the β phase because it was usually quite heavily etched. The α phase however appeared mottled probably as a result of clustering of Cu atoms to relieve supersaturation.

The boundaries in Figs. 23, 25 reveal a distinct tempering effect. Here the original boundary is marked by the termination of the dislocations ahead of which has grown, G.P. zone free α. Selected area diffraction patterns taken at the interface did not reveal any orientation difference between the original α and that formed on tempering. For all interfaces observed, the orientation of the α and β phases were of the Kurdjumov-Sachs type.

(b) The isothermally formed precipitate: The Widmanstatten precipitate formed on tempering at 500°C for 1 min. is shown in Fig. 26. It was believed that the morphology of the precipitate is needle like. Figs. 27, 28 and 29 show the general morphology of the tips of the plates observed. The long sides of the plates were generally smooth with only the occasional step. As the interface curved in towards the tip of the plate, however, the step density increased with increasing deviation from the regular habit. Each ledge appeared to contain a dislocation. The lower side of the plate in Fig. 27 shows a "dot contrast" affect, characteristic of dislocations approximately perpendicular to the plane of the foil. The dislocations at the ledges in Fig. 29 are trailing the interface in the α phase. A very distinct Moire pattern at the interface in Fig. 28. The Kurdjumov-Sachs relation was again found for this precipitate.

These phase boundaries did not move on tempering; instead the α precipitated independently from the retained β in the form of cuboids as shown in Fig. 30.

(c) Trace analysis: The habit plane, predicted by the W-L-R theory for the precipitation of Widmanstatten α from β-brass was calculated. Extrapolating the results of Beck and Smith, the lattice parameters of the α and β phases in the alloy used are a_o^α = 3.702Å a_o^β = 2.948Å at 30°C. Using 20.8 x 10^{-6}/C° for the linear coefficient of thermal expansion for α brass and 24.0x 10^{-6}/C° for β-brass these lattice parameters at 500°C, a_o^α = 3.738Å, a_o^β = 2.981Å. The habit plane calculated from these values is:

$$\begin{matrix} -.2712 \\ .9736 \\ .6892 \end{matrix}$$

corresponding to a relative volume of V = 0.98614.

The habit plane for precipitate formed at 200°C was not calculated because of the uncertainty of phase boundary compositions at that temperature.

The habit plane at 200°C, however, should not be far removed from that predicted at 500°C.

A trace analysis of facets formed is presented in Fig. 31. The predicted value of the habit plane is plotted as a line segment parallel to the c/a = 1 curve (Fig. 3), because of errors in lattice parameters resulting from the use of extrapolation and expansion coefficients.

The experimental value of the habit plane is plotted as the points of intersection of traces of both 500°C and 200°C facets and is in good agrement with the W-L-R predicted value.

CHAPTER 6

Discussion

The electron microscope has found its greatest use in the study of fine-scale precipitation, and, in one case, controlled coarse Widmanstatten precipitation[35]. However the fact that many theories of precipitate morphologies are based on the microscopic nature of the precipitate-matrix interface has led to this investigation using randomly oriented foils. This method, although time consuming, appears to be the most satisfactory way to investigate interfacial structure.

6.1 The Massive Transformation

The microstructural detail found in the $\beta' \rightarrow \alpha$ massive reaction (figure 11) appears to be similar to the massive transformation in Cu-Ga alloys as reported by Saburi and Wayman[64]. Although the massive reaction proceeds via the migration of an incoherent interface, the habit planes observed in the quenched transformation product are close to those predicted by martensite phenomenological theory. It is possible that these habits represent the slowest growing orientations. By analogy to crystal growth from liquids, the rapidly growing faces would disappear, leaving behind a crystal bounded by slow growing planar boundaries. A short planar segment is evident in the β-α boundary of figure 11.

The sub-boundary structure in the massive α phase tempered at 200°C for 3 hrs. appears faceted. This observation, while of limited scope, is consistent with Mott's hypothesis[18].

6.2 Precipitation in 54.5% Cu Brass

The micrographs of this alloy, tempered at 200°C for 24 hrs. indicate that a plate-like precipitate has formed. The microstructure in the as quenched alloy accompanied by diffuse streaking in <211> is probably the result of matrix coherency strains in very early stages of precipitation.

The maxima that occur on these streaks after tempering plus the gradual fading of the streaks themselves presents a problem not readily solvable with the diffraction information obtained. There are three distinct possibilities

1. The maxima result from the addition of the diffracted intensity from the precipitate plus the diffuse intensity (due probably to the effect of precipitate shape). The precipitate spots are too faint to be seen other than on the diffuse streaks. This interpretation would yield a precipitate unit cell with a lattice parameter of ∿8.85Å (cf. γ-brass). However the pattern is not consistent with a simple three-fold increase in the basic repeat distance.

2. The maxima result from the intersection of other streaks not in the plane of the diffraction pattern. This would result from a multiplicity of precipitate habit planes.

3. The maxima are satellites, indicating a modulated structure with an extremely short wavelength.

The author is inclined to favor the second possibility although a firm statement would require further intensive study. The essential point is that the amount of precipitate observed is not in agreement with the fact that this alloy is only slightly supersaturated on quenching in accordance with the Cu-Zn phase diagram Fig. 5(a). Thus the possibility of a eutectoid decomposition of the β phase is suggested.

6.3 Precipitation in the Cu-Zn-Sn Alloy

The morphologies observed indicate that the $\beta \rightarrow \gamma$ reaction in this alloy is analogous to "dendritic" solidification. Since all orientation relationships between precipitate and matrix were of the kind shown in Fig. 18, we must infer that growth of a nucleus formed with any other orientation relationship would be less probable because of a large value of the surface tension. This "ideal" orientation relationship is consistent with that reported by Woo, Barrett and Mehl.

Once this orientation relationship is obtained, the precipitate can evidently grow into the matrix with the precipitate-matrix interface assuming any possible spatial orientation. Thus for this particular condition the surface tension is isotropic to a first approximation.

In this isotropic system, precipitate growth proceeds unrestricted, controlled only by long range matrix diffusion of Sn. The composition ratio of copper and zinc was found to be constant across the precipitate matrix

interface suggesting that this reaction can be considered to proceed in a pseudo binary system. The regularity of the secondary dendrite arm spacing is also indicative of diffusional co-operative growth.

In Fig. 15(b) the onset of growth of secondary branches from the main branch is shown. Although not all the contrast effects in this micrograph can be explained the secondary branches show a definite Ostwald ripening (coarsening) effect. Both the wavelength and amplitude of these perturbations apparently increase with time. The area around the precipitate shows vacancy loop contrast, probably as a result of coalescence of vacancies created by the diffusion of Sn atoms.

The interfacial dislocation arrays (figure 16) suggest that the precipitate, in the early stages at least, is partially coherent with the matrix. In Fig. 16 it is believed that the large precipitate is below the foil surface so that interfacial dislocations can be observed, while the small precipitate has been partly etched through. This leads to the conclusion that there is a minimal increase in surface energy through coherency strains thus there must be extremely good lattice matching.

In view of the growth isotropy of this precipitation it seems reasonable that the Mullins and Sekerka perturbation method[37] could be used to obtain a quantitative value for the surface tension. For a planar interface they found that perturbations must reach a critical wavelength λ_o given by:

$$\lambda_o = 2\pi\left\{\frac{\Gamma_D D C_o}{(v (C-C_s)}\right\}^{1/2} \qquad (6.1)$$

where D = diffusivity of solute in the matrix

C_o = equilibrium concentration of the interface

C_s = concentration at a general interface

C = concentration of solute in the precipitate

v = the velocity at which each element in this interface moves.

Γ_D = a capillary constant $\frac{\gamma\Omega}{RT}$ where γ is the interfacial free energy and Ω the increment of precipitate volume per mole of added solute.

The wavelength λ_M corresponding to maximum growth rate is given by:

$$\lambda_M = \sqrt{3}\,\lambda_o \tag{6.2}$$

Mullins and Sekerka's equations apply only to cases where the concentration of solute in the precipitate is much greater than that in the matrix. In our particular case of $\beta \rightarrow \gamma$ precipitation the supersaturation is quite high so all that can be expected, at best, is an order of magnitude for the surface tension.

The values used for equation (6.1) were:

1. $\Omega = \frac{\text{atomic weight Cu}}{\text{density of Cu}} = 7.15$ cc/mole

2. $D_{Sn} = 1.2 \times 10^{-12}$ cm^2/sec. (calculated from the thickness of the precipitate in Fig. 19(a)).

3. The V measured from Fig. 19(a) was multiplied by a factor of 4 to account for rapid intial growth giving $V = 1.5 \times 10^{-7}$ cm/sec.

4. Since the Cu/Zn ratio was constant the tie lines could be approximately determined. This tie line intersected the $\gamma/\gamma + \beta$ phase boundary

at approximately 8% Sn. Because the Mullins and Serkerka analysis requires one phase to be pure the compositions were referred to as % (8% Sn) giving $C_o = C_s = .3$ and $C - C_s = .7$.

Substituting a value of 100 ergs/cm^2 into eqn. 6.1 one obtains a value of 226Å for λ_M. This value is within a factor of two of the measured wavelength of ∿400Å. Although the approximations used are very rough this result does indicate that a low value of surface tension does account for the observed morphology. Since there is excellent lattice matching of the two phases the boundary in the adjacent grain (figure 19) can be considered as a high angle β-β type with a typical energy value of ∿500 - 1500 ergs/cm^2. It is interesting to note that, for this grain boundary precipitate case, the precipitate grew into the grain with which it shared an ideal orientation relationship. This observation can be rationalized on the basis of the widely differing surface tensions involved. It would be of great interest to test the validity of the "classical" ideas of C.S.Smith[22] in other more conventional systems.

6.4 Widmanstatten Precipitation

(a) Precipitate formed on continuous cooling: Because the interfaces of the as quenched precipitate appeared smooth, and the interfaces of the tempered precipitate exhibited microscopic facets, it is inferred that the interface migrational characteristic is different in the two cases. Since the time spent at the optimum growth temperature during the quench is ∿0.1 seconds, the interface would have to propagate by a

"near-massive" mechanism to give the observed precipitate size (Fig. 20). Here the local driving force for transformation must be large so that non-conservative (i.e. defect producing) motion is energetically feasible.

Tempering at 200°C brought about interface migration due to the lack of fine scale precipitation in the β-phase. During the latter stages of the tempering operation, the large driving force implied for the continuous cooling case was absent.

The boundary, now, must migrate only to relieve the local supersaturation of the retained β phase at the interface. At late stages in diffusional reactions, this supersaturation must be extremely small.

The interface formed on quenching is seen in Figs. 23 and 25 to be marked by a line of dislocations. This boundary has migrated during tempering, forming α phase which exhibits a different contrast than the original α. In Fig. 25, the dislocations in the as-quenched α phase appear to be pinned, probably as a result of Guinier-Preston zone formation to relieve supersaturation in this phase. The equilibrium α phase, formed on tempering is free of these G-P zones.

The faceted structure of the α-β interfaces formed on tempering provides strong support for the argument of Cahn (sec. 2.7). i.e. for conditions corresponding to insufficient driving force for "normal" boundary movement, migration must proceed via a two dimensional nucleation, ledge motion mechanism. In other words, boundary structure and migration mechanism is a function of imposed thermodynamic conditions.

It was found that, within the limits of experimental error, all of the facets were consistent with the habit plane predicted by a minimum interfacial strain energy criterion. Thus it is inferred that the interfacial strain component of the surface energy is a strong force tending to stabilize planar interfaces. Thus for Kurdjumov-Sachs oriented phases, it is perhaps not surprising that the martensite habit plane and the isothermal precipitation habit plane are both given by the W-L-R theory.

The complicated array of dislocations trailing the interface in Fig. 25 would appear to be the result of imperfect reconstruction of the growing crystal lattice from an incoherent boundary (note dislocation spirals in Fig. 25, suggesting defect condensation) and not as a result of non-conservative interfacial dislocation motion. However, this point would benefit from further detailed investigation.

(b) The isothermally formed precipitate: The high density of ledges in the Widmanstatten precipitate formed isothermally, lend further support to the minimum strain energy criterion for these interfaces. As the radius of curvature increases at the tip of the plate (Figs. 27 and 29), the density of steps increases. The interface exhibits no tendency toward assuming a disordered structure. Although a macroscopic equilibrated interface may appear to deviate from the predicted habit it will evidently remain in a faceted configuration. This is best seen in Fig. 27 where two α-β boundaries (one at a curved Widmanstatten tip) yield the same contrast when they are parallel.

It can be stated then, that in Widmanstatten α precipitation when the driving force is small, the boundary between phases is such that the interfacial strain energy is minimized. Thus the strain energy term in the interfacial energy is the dominant one, at least at low temperatures where coherency is considered more probable.

It should be noted that these results apply to late stages in the precipitation reaction; at early times when diffusion control theory predicts infinite rates of growth it is expected that non-conservative interface migrational characteristics will be found.

CHAPTER 7

Conclusions

In the course of this investigation two distinctly different forms of precipitation have been observed and discussed. In each reaction there is a different criterion governing the characteristics of the interface and thus the precipitate morphology (in each case, also a definite orientation relationship must be obtained).

In the $\beta \rightarrow \gamma$ reaction in Cu-Zn-Sn a dendritic precipitate morphology develops as a result of the isotropy of surface tension. The Mullins and Sekerka perturbation method,[37] while not strictly applicable to this case, has indicated that the surface tension associated with $\beta \rightarrow \gamma$ boundaries is low enough to permit a state of interfacial instability to exist.

The $\beta \rightarrow$ Widmanstatten α reaction in brass has been found to assume the habit plane predicted from the martensite phenomenological theory. It can be concluded from this result that for this system the magnitude of strain at the interface is the primary factor in determining the habit. Similar investigations on other alloy systems will have to be carried out in order to test the general validity of this statement.

It has been established that α-β boundaries between Kurdjumov-Sachs oriented phases can be microscopically smooth or faceted. The

observation that the migrational mechanism of the Widmanstatten interface changes with the magnitude of the local driving force is the first experimental evidence found in support of Cahn's theory of interface motion[30]. This observation further suggests that great care should be exercised when considering mechanistic theories of precipitate morphology[22].

REFERENCES

1. Christian, J.W., The Theory of Transformations in Metals and Alloys, Pergamon Press, London (1965).

2. Gibbs, J.W., Collected Works, 1948, 1, Yale University Press.

3. Barrett, C.S., Structure of Metals, McGraw Hill, (1952).

4. Wayman, C.M., Introduction to the Crystallography of Martensite Transformations, McMillian (1964).

5. Dautovich, D., Purdy, G.R., Can. Met. Quart., 4, 129 (1965).

6. Spencer, C.W., AIME Symposium on the Decomposition of Austenite by Diffusional Processes, 549, Interscience, New York (1962).

7. Shapiro, J., Ph.D. Thesis, McMaster University (1966).

8. Kelly, A., Nicholson, R. B., Progress in Materials Science, 10, 151, (1963).

9. Cahn, J.W., Acta Met., 9, 795, (1961).

10. Krivoglaz, M.A., Smirnov, A.A., Theory of Order Disorder in Alloys, American Elsevier Pub. Co., (1965).

11. Zener, C., Trans. AIME, 167, 550, (1946).

12. Cottrell, S.A., Ko, T., J.I.S.I., 173, 224 (1953).

13. Speich, G.R., Decomposition of Austenite, 353, Interscience, New York (1962).

14. Hillert, M., Decomposition of Austenite, 197.

15. Otte, H.M., Massalski, T.B., Acta Met, 6, 494 (1958).

16. Amelinckx, S., Dekeyser, W., Solid State Physics, 8, 327, (1959).

17. Burgers, J.M., Proc. Koninkl. Ned. Akad. Wetenschap, 42, 378, (1937).

18. Mott, N.F., Proc. Phys. Soc., 60, 391, (1958).

19. Shockley, W., Read, W.T., Phys. Rev., 75, 692 (1949).

20. Van der Merwe, J.H., Proc. Phys. Soc., 63A, 613 (1950).

21. Smith, C.S., Trans A.S.M., 45, 533 (1953).

22. Aaronson, H.I., Decomposition of Austenite, Interscience, New York (1962).

23. Smith, C.S., Trans A.I.M.E., 175, 15, (1948).

24. Christian, J.W., Decomposition of Austenite, 371, Interscience (1962).

25. Bever, M.B., Energetics in Metallurgical Phenomena, Gordon and Breach, New York (1965).

26. Brooks, H., Trans A.S.M., 44A, 20, (1952).

27. Smith, C.S., Imperfections in Nearly Perfect Crystals, 377, Wiley, New York (1952).

28. Smith, C.S., Discussion to ref. (14).

29. Burton, W.K., Cabrera, N., Frank, F.C., Phil Trans, 243, 299 (1950-51).

30. Cahn, J.W., Acta Met., 8, 554 (1960).

31. Shewmon, P.G., Robertson, W.M., 67, Metal Surfaces A.S.M. (1962).

32. Kurdjumov, G.V., Sachs, G., Z. Physik, 64, 325 (1939).

33. Paxton, H.W., Journal of Chemical Physics, 26, 1769 (1957).

34. Hren, J.A., Thomas, G., Trans A.I.M.E. 227, 308, (1963).

35. Aaronson, H.I., Laird, C., To be published.

36. Rutter, J.W., Chalmers, B., Can. J. Phys., 31, 15 (1953).

37. Mullins, W.W., Sekerka, R.F., J. Appl. Phys, 34, 323, (1963).

38. Shewmon, P.G., Trans A.I.M.E., 233, 736 (1965).

39. Callen, H.B., Thermodynamics, 231, Wiley (1960).

40. Zener, C., Phys. Rev., 71, 846 (1947).

41. Greninger, A.B., Mooradian, V.G., Trans A.I.M.E., 128, 337 (1938).

42. Hull, D., Garwood, R.D., The Mechanisms of Phase Transformations in Metals, Institute of Metals, London (1956).

43. Bassi, G., Strom, B., Z. Metallkunde, 47, 16, (1956).

44. Hull, D., Garwood, R.D., Acta Met., 6, 98 (1958).

45. Kunze, G., Z. Metallkunde, 53, 329, (1962), 53, 396, (1962).

46. Masson, B.D., Govila, R.K., Z. Metallkunde, 54, 243, (1963).

47. Jolley, W., Hull, D., J.I.M. 92, 129, (1963-64).

48. Titchener, A.L., Bever, M.B., Trans. A.I.M.E., 200, 303, (1954).

49. Massalski, T.B., Barrett, C.S., Trans. A.I.M.E., 209, 455 (1957).

50. Williams, H.D., Smith, G.C., Phil. Mag. 13, 124 (1966).

51. Hull, D., Phil. Mag., 1, 76, (1962).

52. Srinivasan, G.R., Anatharaman J.R.

53. Garwood, R.D., J.I.M., 83, 64 (1954-55).

54. Shinoda, G., Amano, Y., J. Phys. Soc. of Japan, 6, 508 (1951).

55. Woo, S., Barrett, C.S., Mehl, R.F., A.I.M.M.E. Tech. Pub. 1694, (1944).

56. Hu, H., Smith, C.S., Acta Met., 4, 638 (1956).

57. Cox, G.W., Ph.D. Thesis, University of New South Wales, (1965).

58. Shinoda, G., Amano, Y., Trans. Jap. Inst. Met. 1, 54, (1960).

59. Kay, D.H., Techniques for Electron Microscopy, Blackwell, Oxford, (1965).

60. Siemens Elmiskop Manual.

61. Hirsch, P.B., et al, Electron Microscopy of Thin Crystals, Butterworths, London, (1965).

62. Mehl, R.F., Marzke, O.T., Trans. A.I.M.E., 93, 123, (1931).

63. Zener, C., J.A.P., 20, 950, (1949).

64. Saburi, T., and Wayman, C.M., Trans. A.I.M.E., 223, 1373, (1965).

TABLE 1

Properties of α, β and γ Brass

Property	α - Brass	Beta Brass	γ - Brass
Structure	fcc - solid solution Order disorder reaction at 700°C at Cu_3Zn	bcc - 3/2 electron Compound β at >450° disordered bcc β' <450°C $L2_0$ type superlattice	Cubic $D8_2$ 21/13 electro compound
Lattice parameters	3.64 at % Zn 18°C-3.6218 Å 34.25% Zn 18°C-3.6923 Å	β' 47.66 at % Zn a = 2.9539 Å	at Cu_5Zn_3 a = 8.857 Å
Density	30% wt Zn 8.52 gm/cc	at CuZn 8.20 gm/cc	
Elastic properties			
$\frac{E_{111}}{E_{100}}$	4.0	8.9	
C_{44}	0.72×10^{-12} cm^2/dyne	1.73×10^{-12} cm^2/dyne	
$\frac{C_{11}-C_{12}}{2}$	0.18×10^{-12} cm^2/dyne	0.093×10^{-12} cm^2/dyne	
Slip system	{111} <110>	{110} <111>	
Stacking fault energy	5 ergs/cm^2		

TABLE 2

Spectrographic Analysis of Alloys

ELEMENT	ALLOYS 60.4% Cu 39.6% Zn	54.5% Cu 45.5% Zn	56.5% Cu 39.5% Zn 4.0% Sn
Sb	<.005%	<.005%	<.005%
As	<.01 %	<.005%	<.01 %
Bi	<.0005%	<.0005%	<.0005%
Cd	<.005%		<.005%
Co	.0005%	.0005%	.0005%
Pb	.0005%	.002%	.001%
Mn	.0005%		.0005%
Ni	.0005%	.0005%	.0005%
Ag	<.0005%	.001%	<.0005%
Sn	.0005%	<.0005%	
Al	.001%	.001%	.005%
Fe	.001%	.002%	.05%
Mg	.001%	.001%	.001%
Si		.005%	

TABLE 3

Heat Treatment Schedule

Composition	Initial Heat Treatment	Subsequent Isothermal Treatment	Remarks
60.4 wt% Cu 39.6 wt% Zn	Equilibrated at 750°C for 1 min. Ice brine quench	1) None 2) 60 min at 200°C	Widmanstatten α growth on quenching To produce phase boundary migration
60.4 wt% Cu 39.6 wt% Zn	Equilibrated at 800°C for 1 min Ice brine quench	1) Tempered at 500°C for 1 min. 2) 500°C for 1 min→ 200°C for 60 min. 3) Tempered 200°C for 60 min.	Extensive Widmanstatten α network. To produce phase boundary migration. Extensive bainite network.
60.9 wt% Cu 39.6 wt% Zn	Equilibrated at 800°C for 1 min. Water quench	1) None 2) Tempered 200°C for 3 hrs.	Massive α produced on quench
54.5 wt% Cu 45.5 wt% Zn	Equilibrated at 700°C for 1 min. Ice brine quench	1) None 2) 24 hrs at 200°C	Large grained beta phase.
56.5% Cu 39.5% Zn 4.0% Zn	Equilibrated at 800°C for 1 min Ice brine quench	1) None 2) 29 hrs. at 200°C 3) 7 min. at 300°C 4) 15 min at 300°C 5) 30 min. at 300°C	Dendritic precipitate formation in a large grained beta.

Fig. 1. CLASSIFICATION OF PHASE TRANSFORMATION

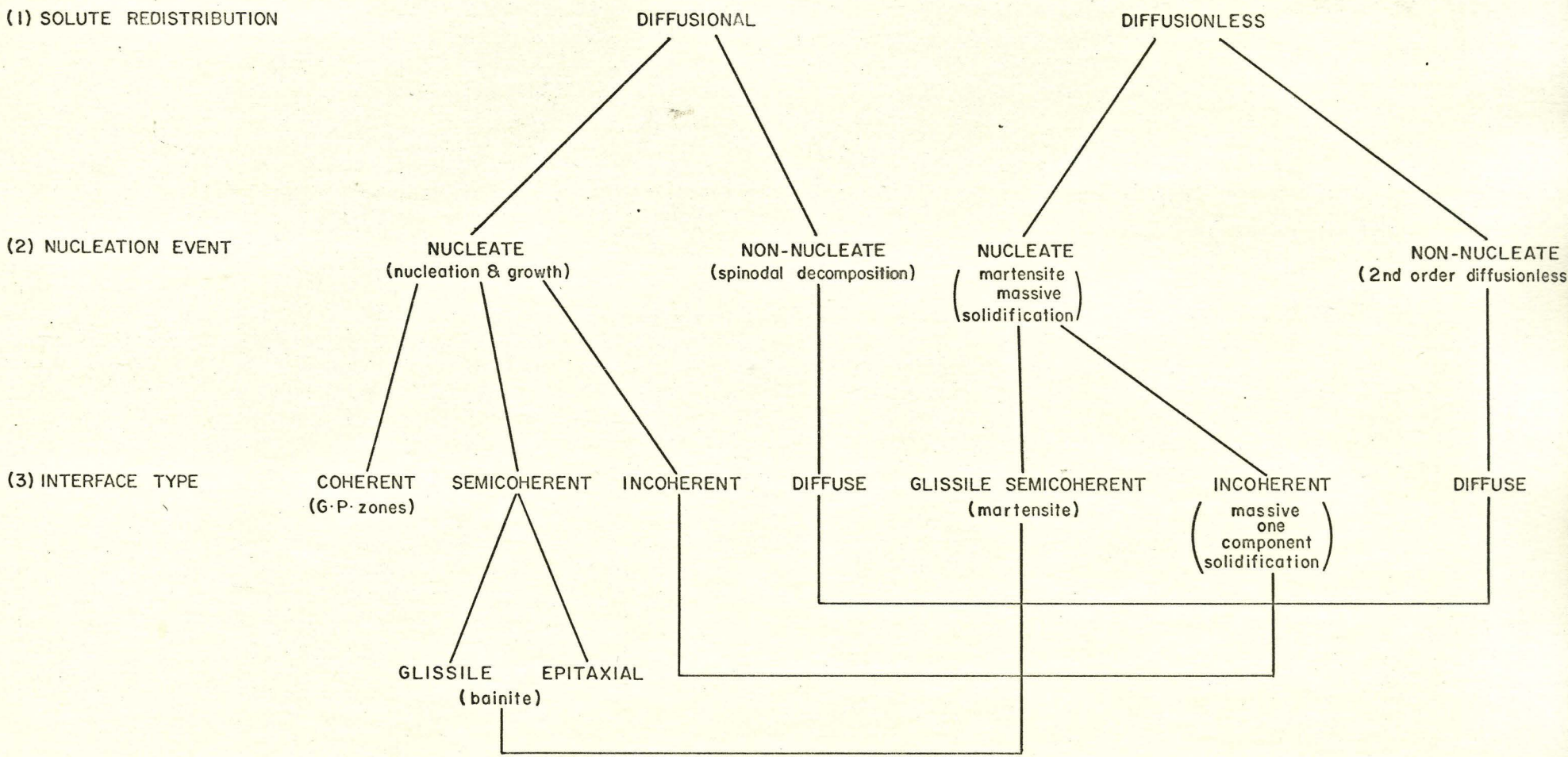

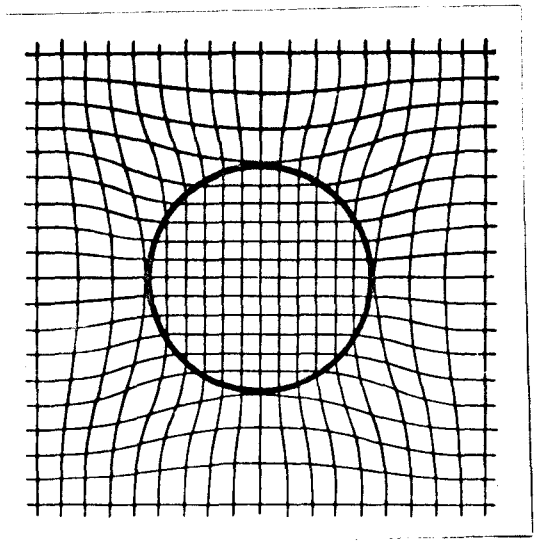

Fig. 2(a) A coherent spherical particle.

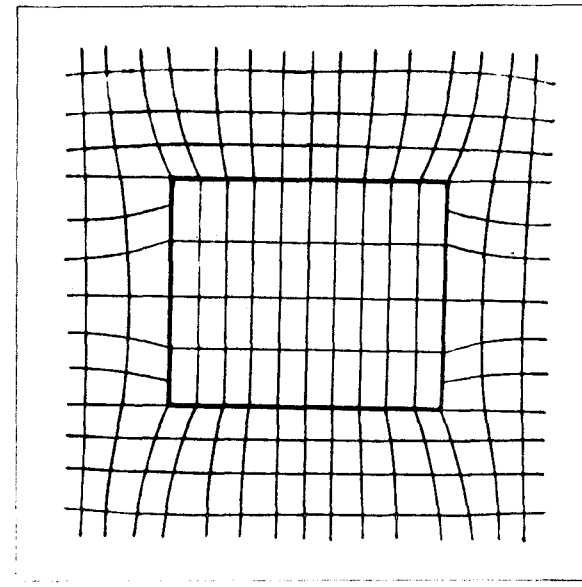

Fig. 2(b) Particle showing two coherent and two semicoherent interfaces

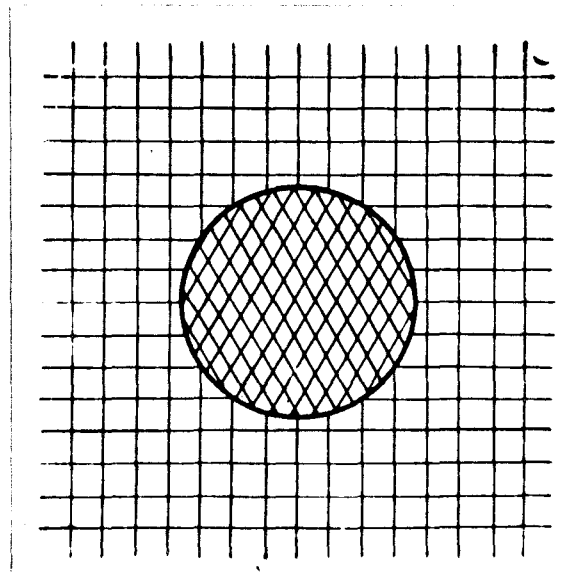

Fig. 2(c) A incoherent Particle

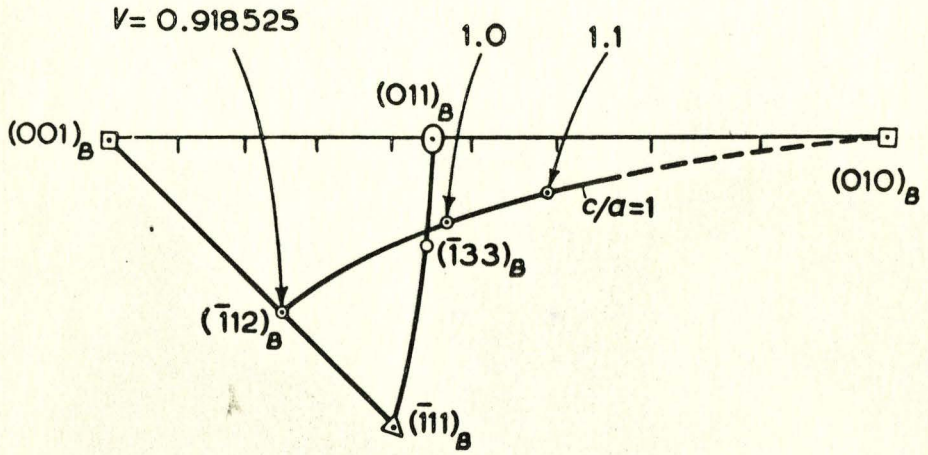

Fig. 3 Variation of the habit plane (hkl) with the relative volume (V) for the bcc⇌fcc transformations.
(from Otte H.M. and Massalski, T.B.[15])

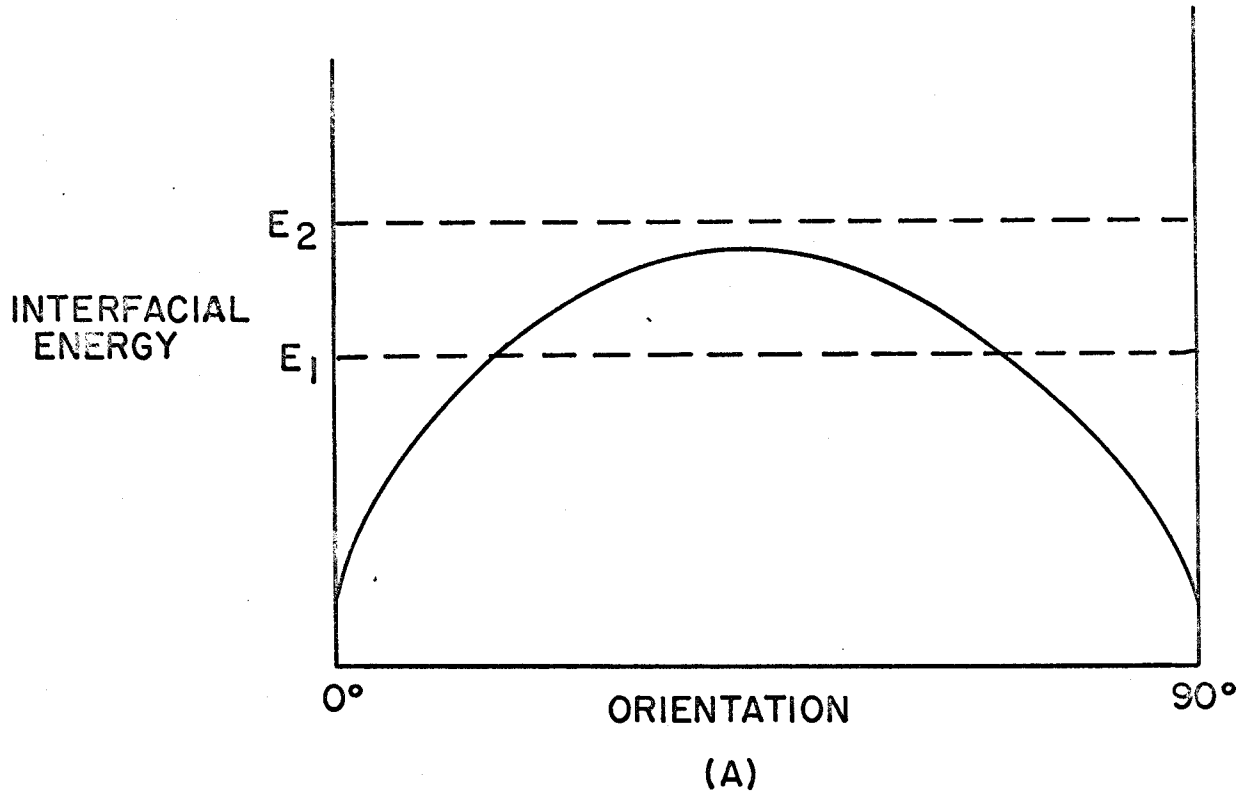

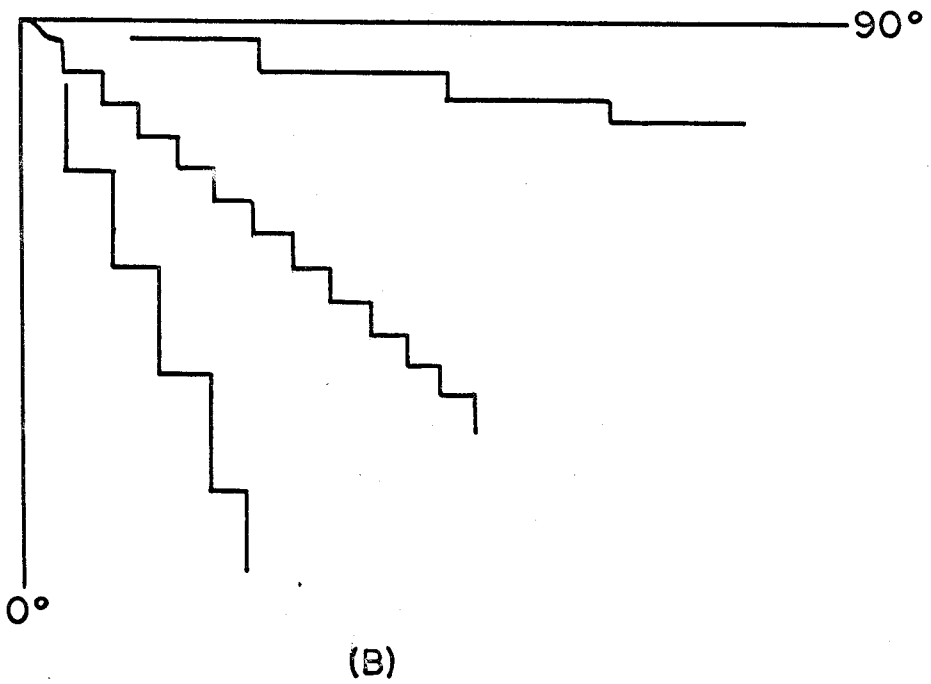

Fig. 4 (a) Variation of Interfacial Energy with Relative Orientation for Two Low Energy Crystallographically Equivalent Interfaces 90° Apart.

(b) Variation of Step Density with Orientation.

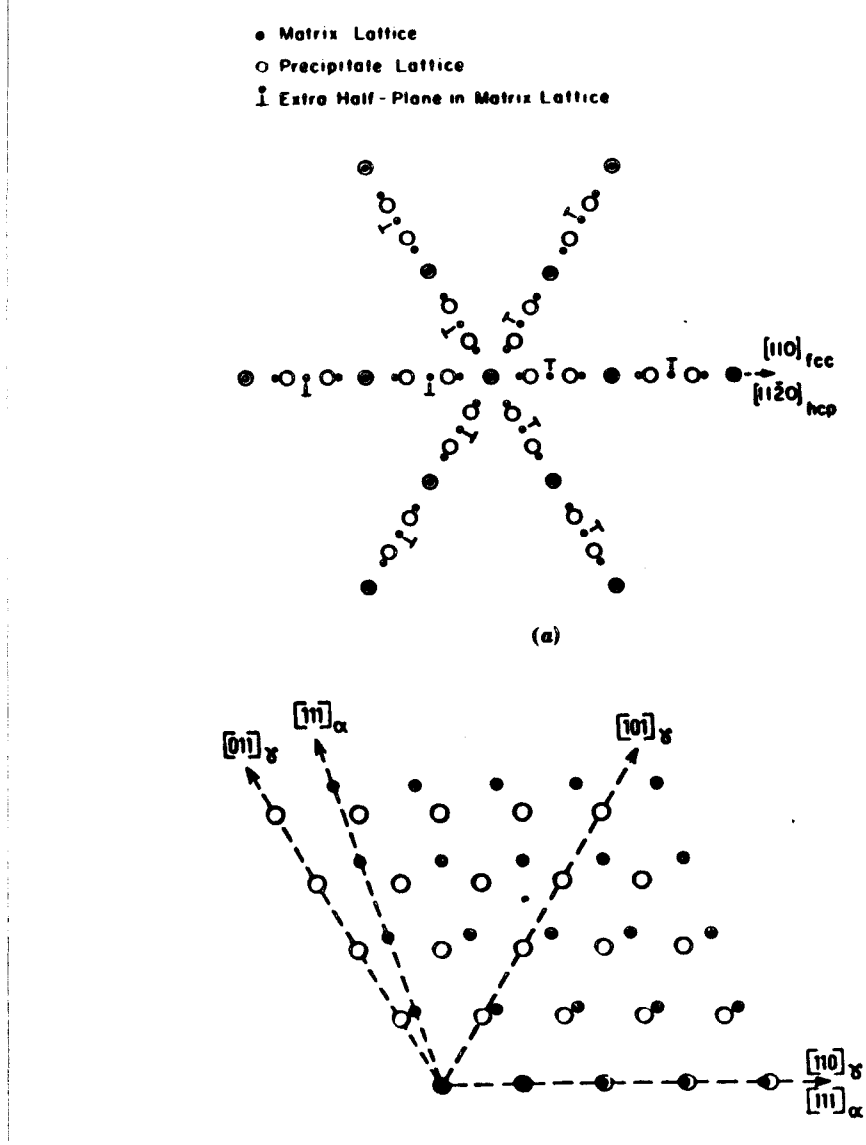

Fig. 5 (a) Structure of the interphase boundary defined by $(111)_{fcc} \parallel (0001)_{hcp}$ and $[110]_{fcc} \parallel [11\bar{2}0]_{hcp}$. (b) Structure of the austenite: ferrite defined by the Kurdjumov Sachs relationships. (after Aaronson[22]).

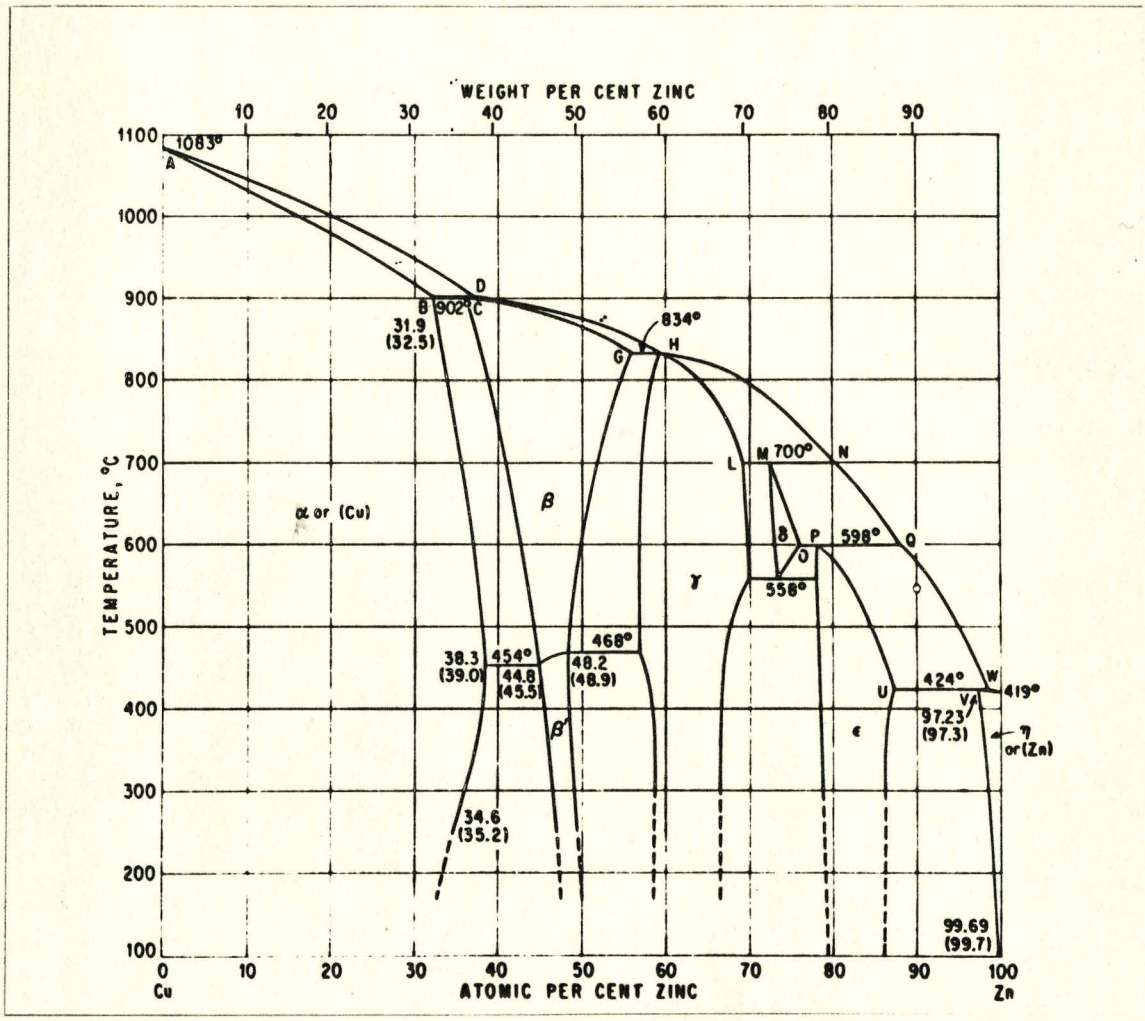

Fig. 6(a) Cu-Zn Phase diagram (ref. Hansen, M. Constitution of Binary Alloys, McGraw Hill, 1958).

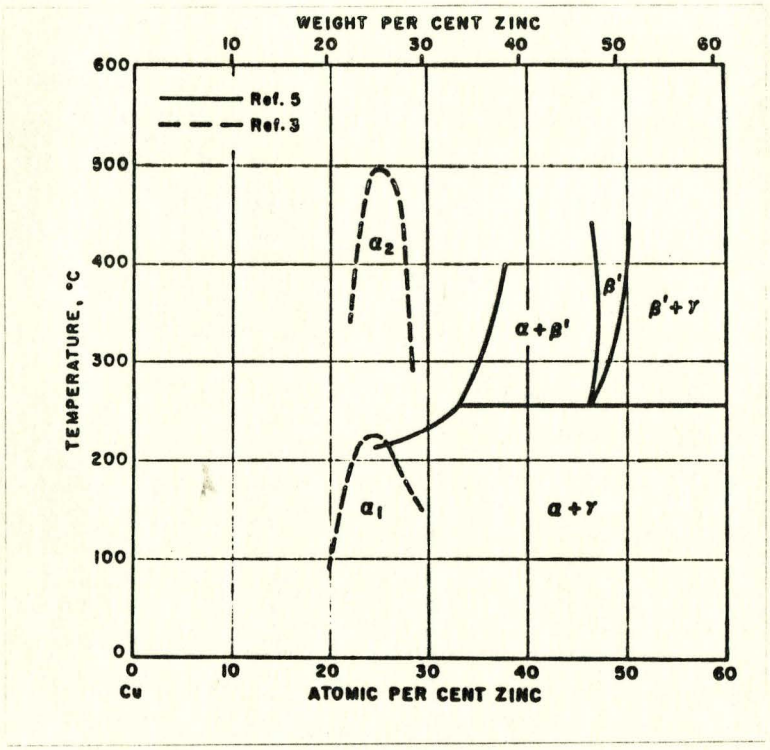

Fig. 6(b) Supplement to Cu-Zn phase diagram

(from Elliott, R.P., Supplement to the Constitution of Binary Alloys, McGraw Hill, 1965)

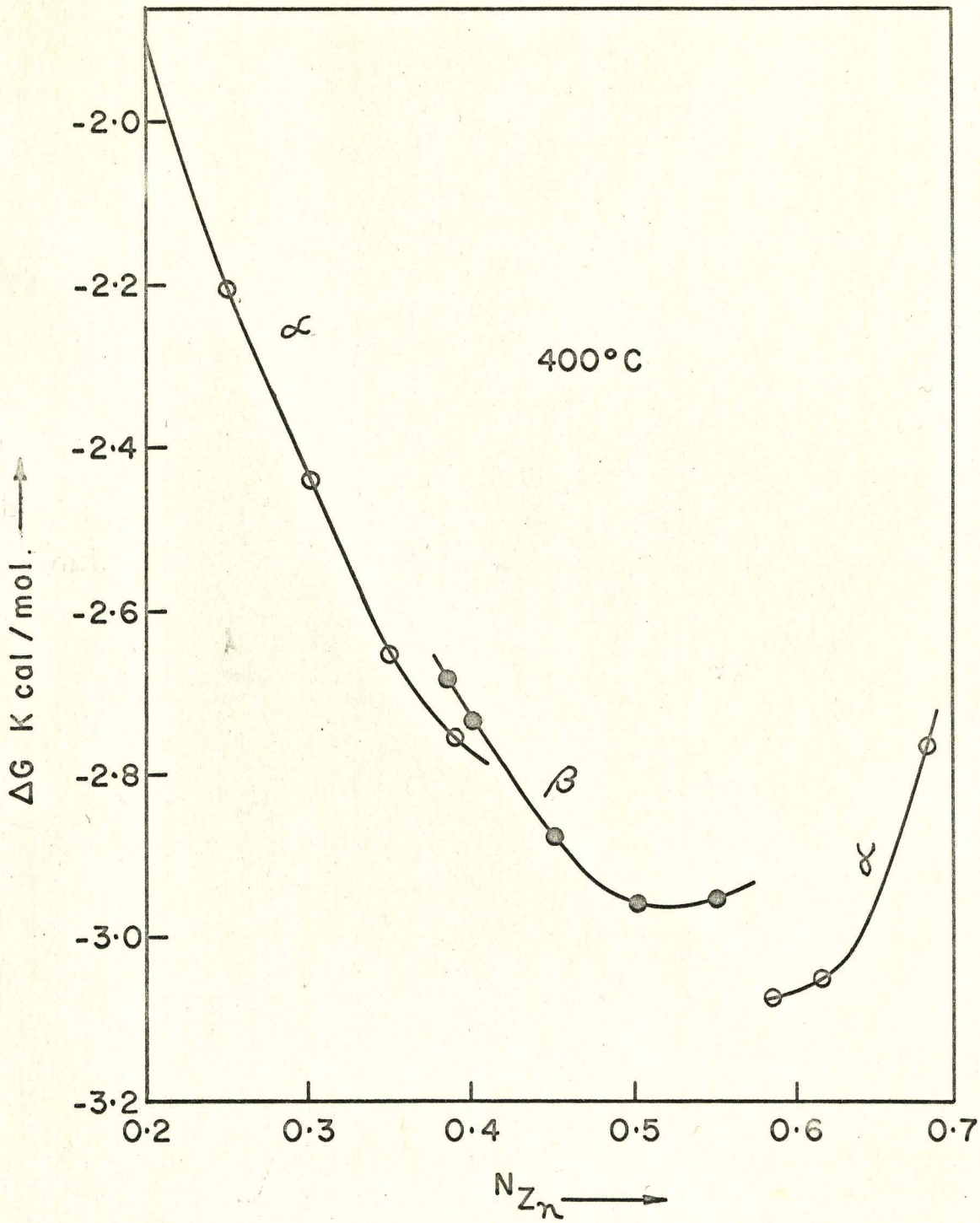

Fig. 7 Free-energy of formation of Cu-Zn alloys vs. mole fraction at 400°C. (after Cox, G.W.[57]).

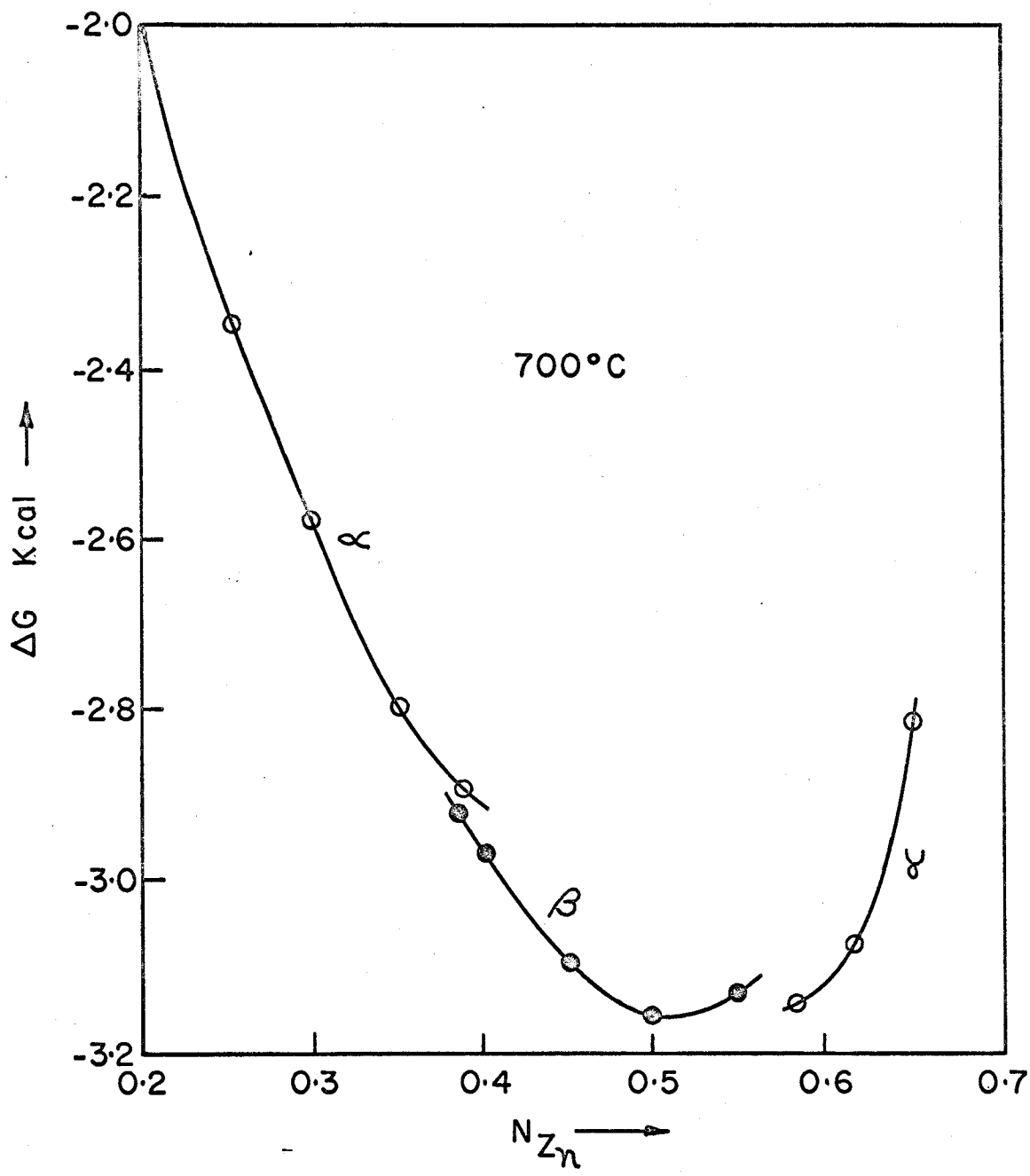

Fig. 8 Free-energy of formation of Cu-Zn alloys vs. mole fraction at 700°C (after Cox, G.W.[57]).

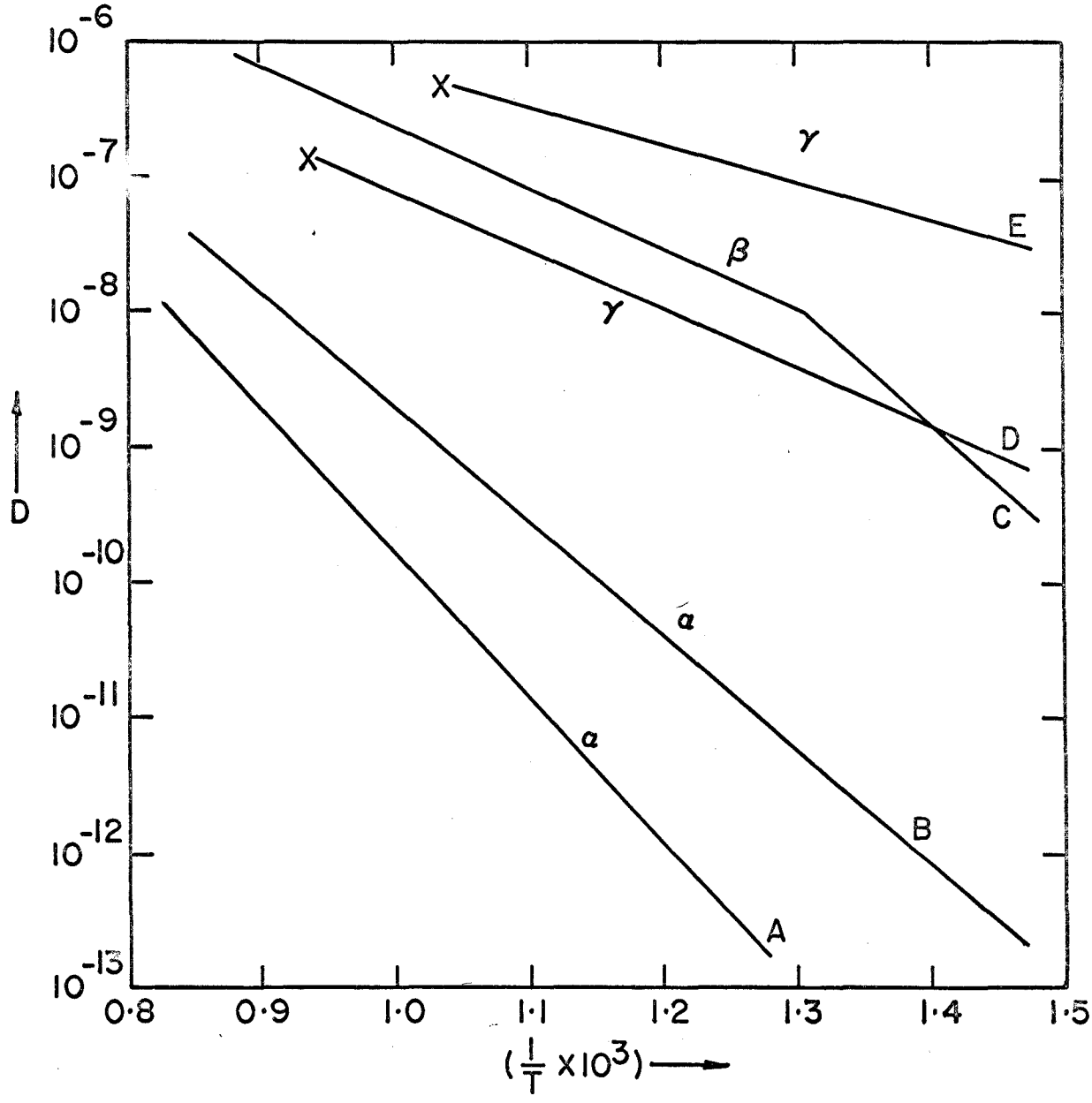

Fig. 9 Chemical diffusion coefficients of the α, β and γ phases of the copper-zinc system, as a function of temperature (after Cox, G.W.[57]).

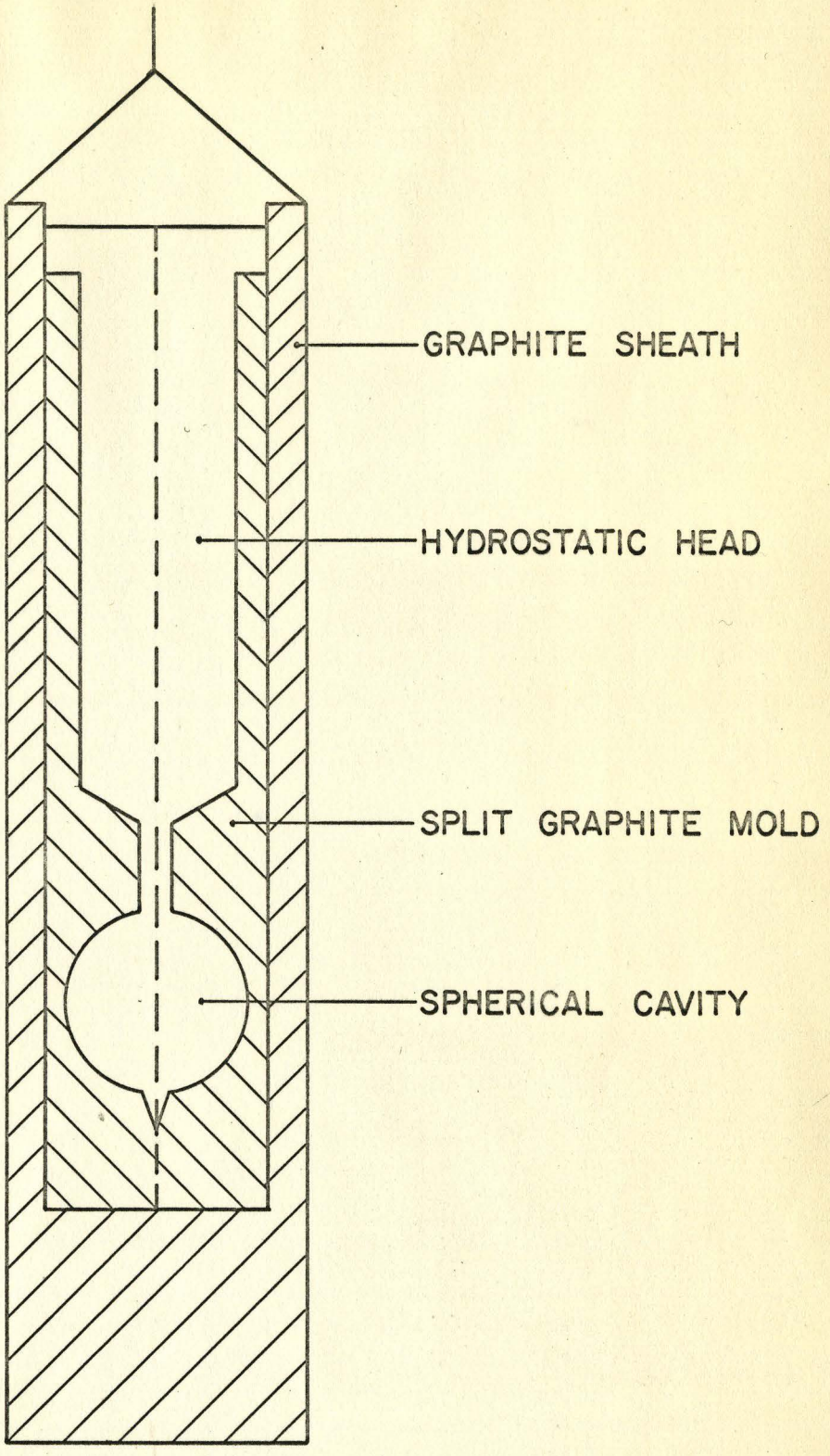

Fig. 10. CRYSTAL GROWING MOLD

Fig. 11 α Massive phase X 26,000

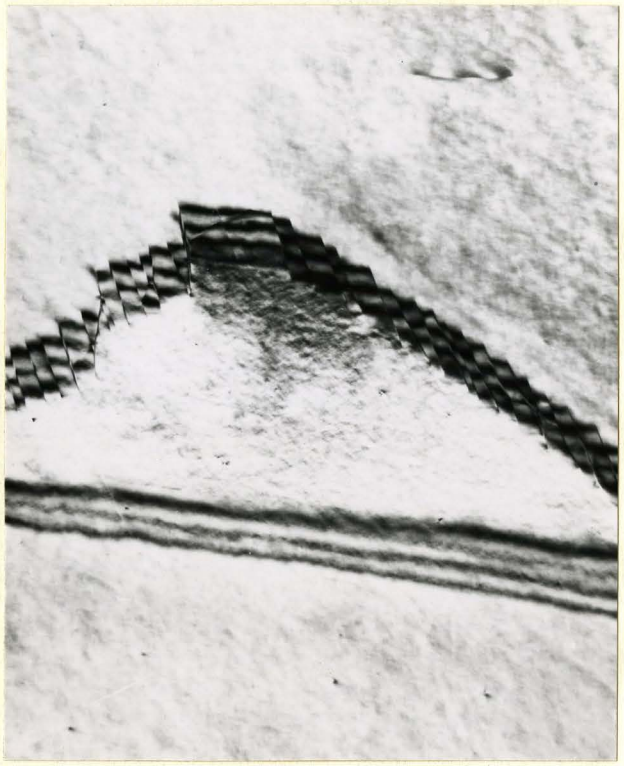

Fig. 12(a) Subgrain in α Brass. X60,000

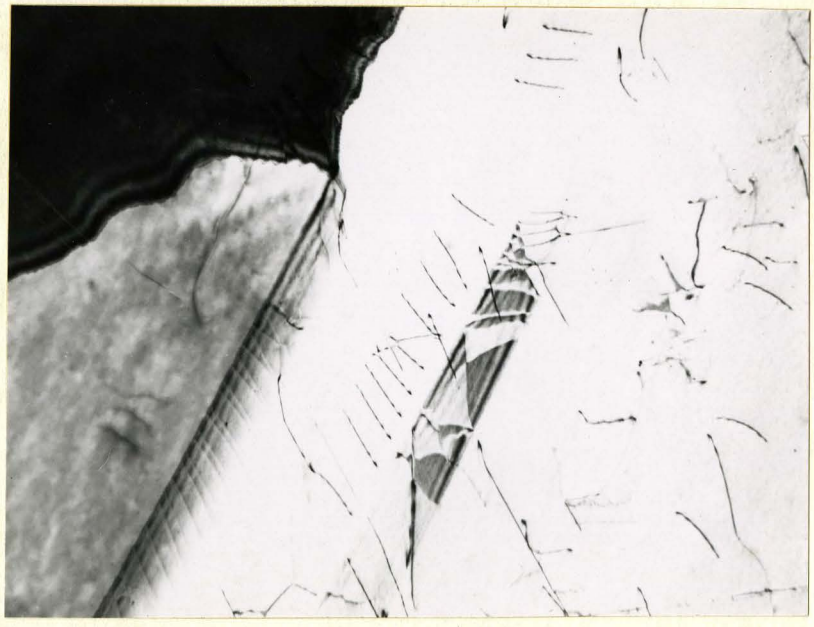

Fig. 12(b) Three grain junction showing boundary facets
X 30,000

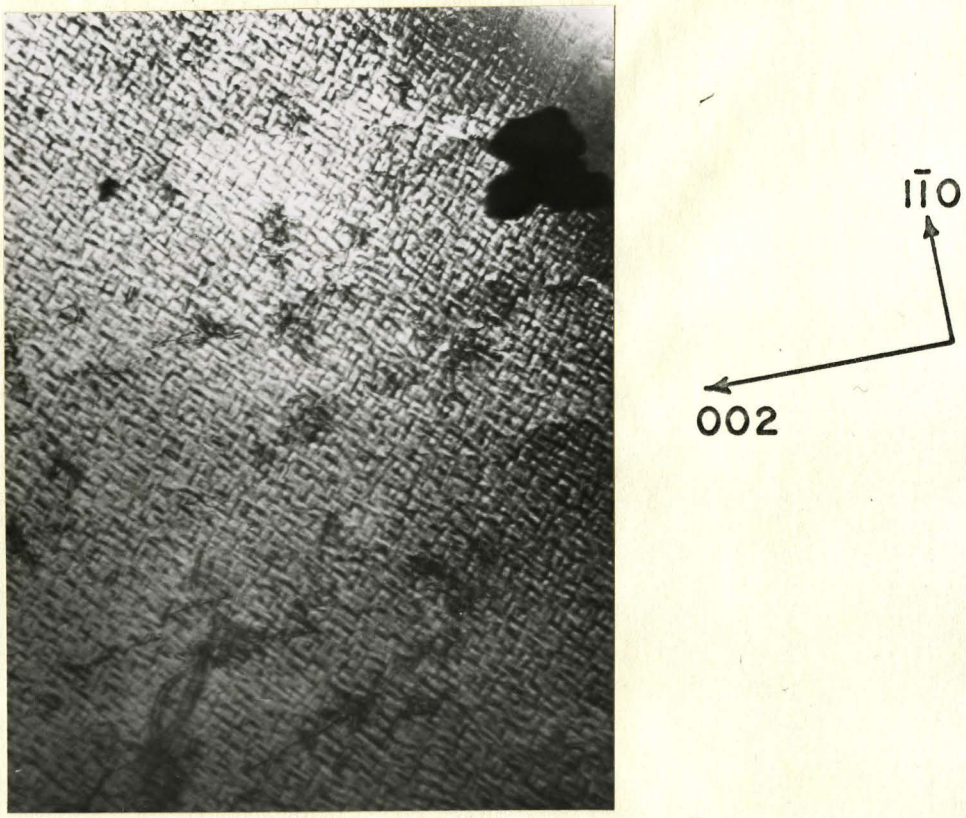

Fig. 13 56.5% Cu in as quenched condition X 30,000

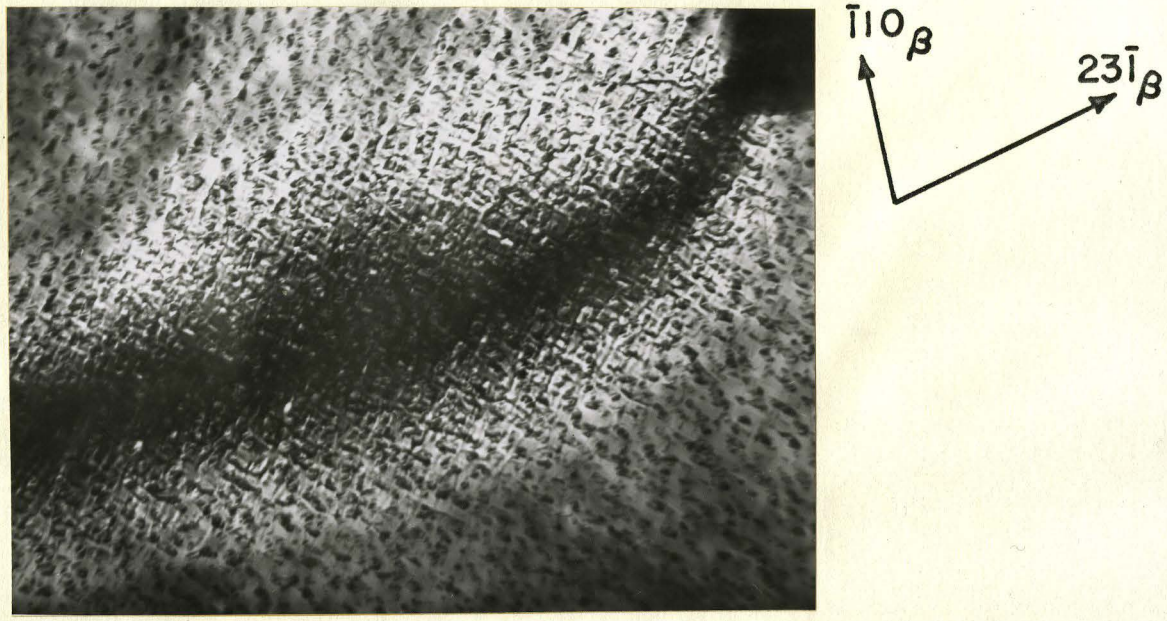

Fig. 14(a) Extinction contour in 56.5% Cu brass. Tempered 24 hrs. at 200°C. X 30,000

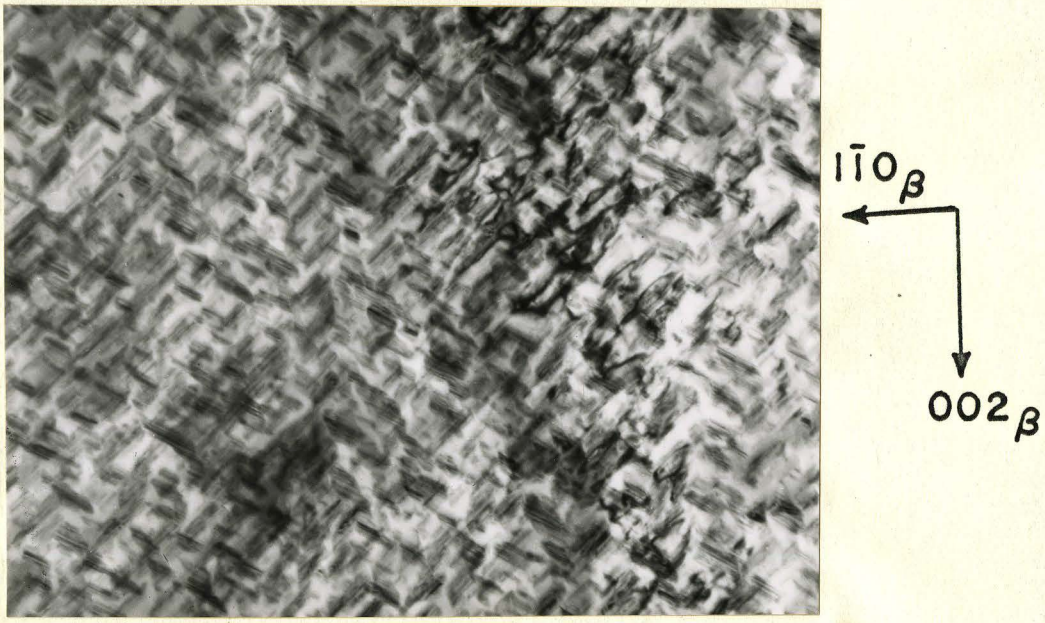

Fig. 14(b) Structure showing displacement fringe contrast in brass. Tempered 24 hrs. at 200°C. X 40,000

Fig. 15(a) Dendritic γ precipitate in Cu-Zn-Sn alloy. Tempered for 7 min. at 300°C. X 30,000

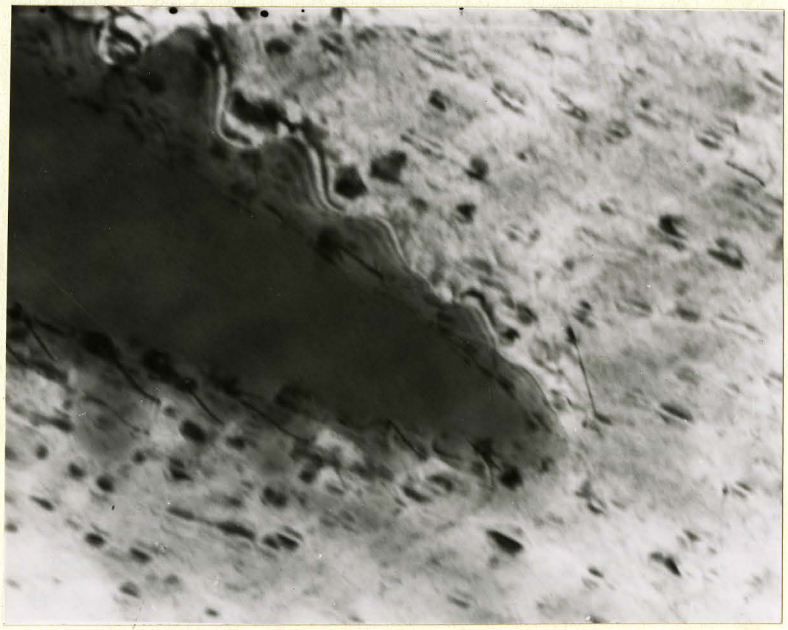

Fig. 15(b) Tip of lower dendrite arm of 15(a) X 95,000

Fig. 16 γ precipitate in Cu-Zn-Sn alloy.
Tempered for 15 min. at 300°C. X 30,000

Fig. 17 γ precipitate in Cu-Zn-Sn alloy
Tempered for 30 min. at 300°C. X 22,000

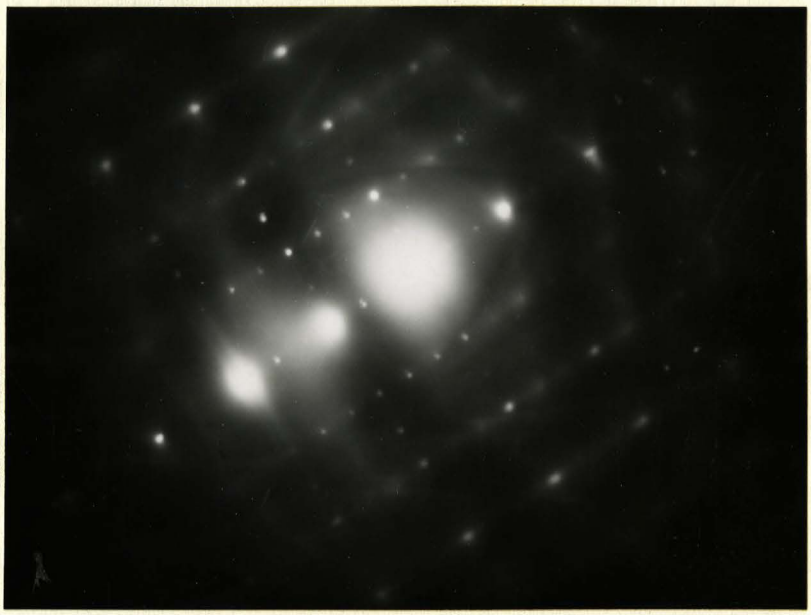

Fig. 18 Typical diffraction pattern of matrix
(large spots) and precipitate (Tilted from 111)

Fig. 19(a) Grain boundary precipitate in Cu-Zn-Sn alloy
Tempered 15 min at 300°C X 30,000

Fig. 19(b) Grain Boundary precipitate in Cu-Zn-Sn alloy
Tempered 15 min. at 300°C X 30,000

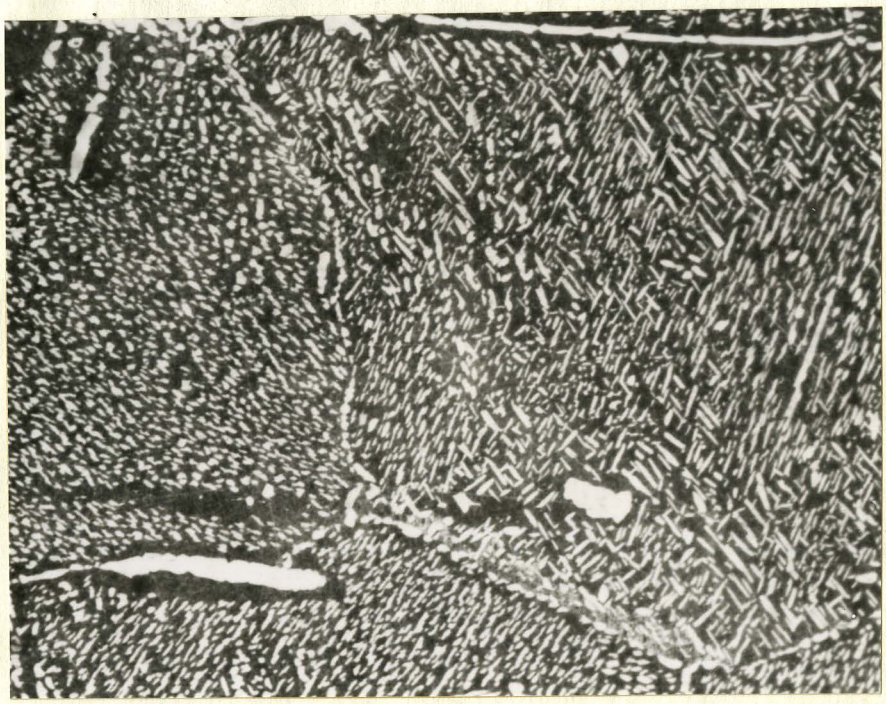

Fig. 20. Widmanstatten α precipitate formed on continuous cooling from 750°C. Copper Ammonium chloride etch. X 150

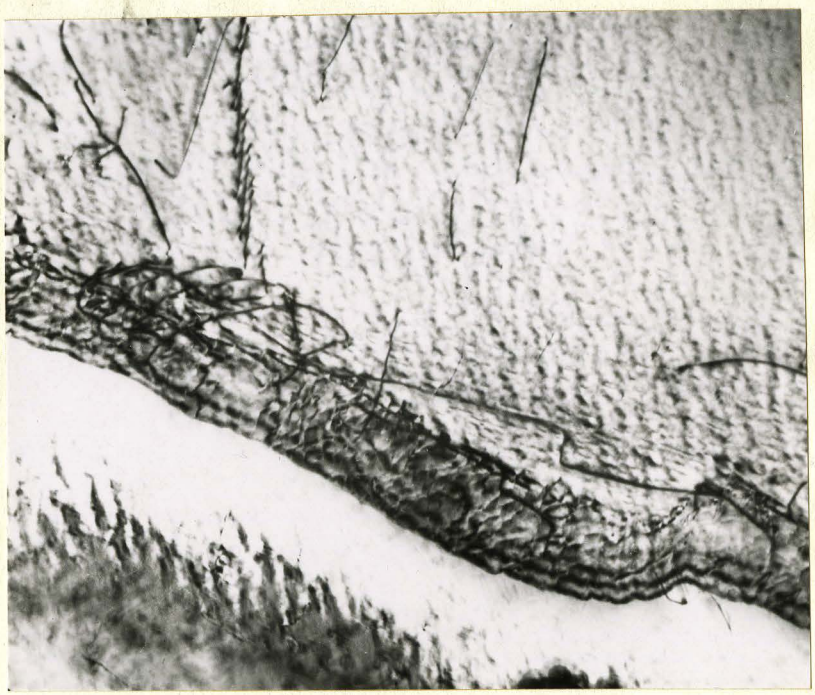

Fig. 21. Widmanstatten α-β interface formed by quenching from 750°C and tempering at 200°C for 1 hr. Note boundary facets and dislocation structure. X 60,000

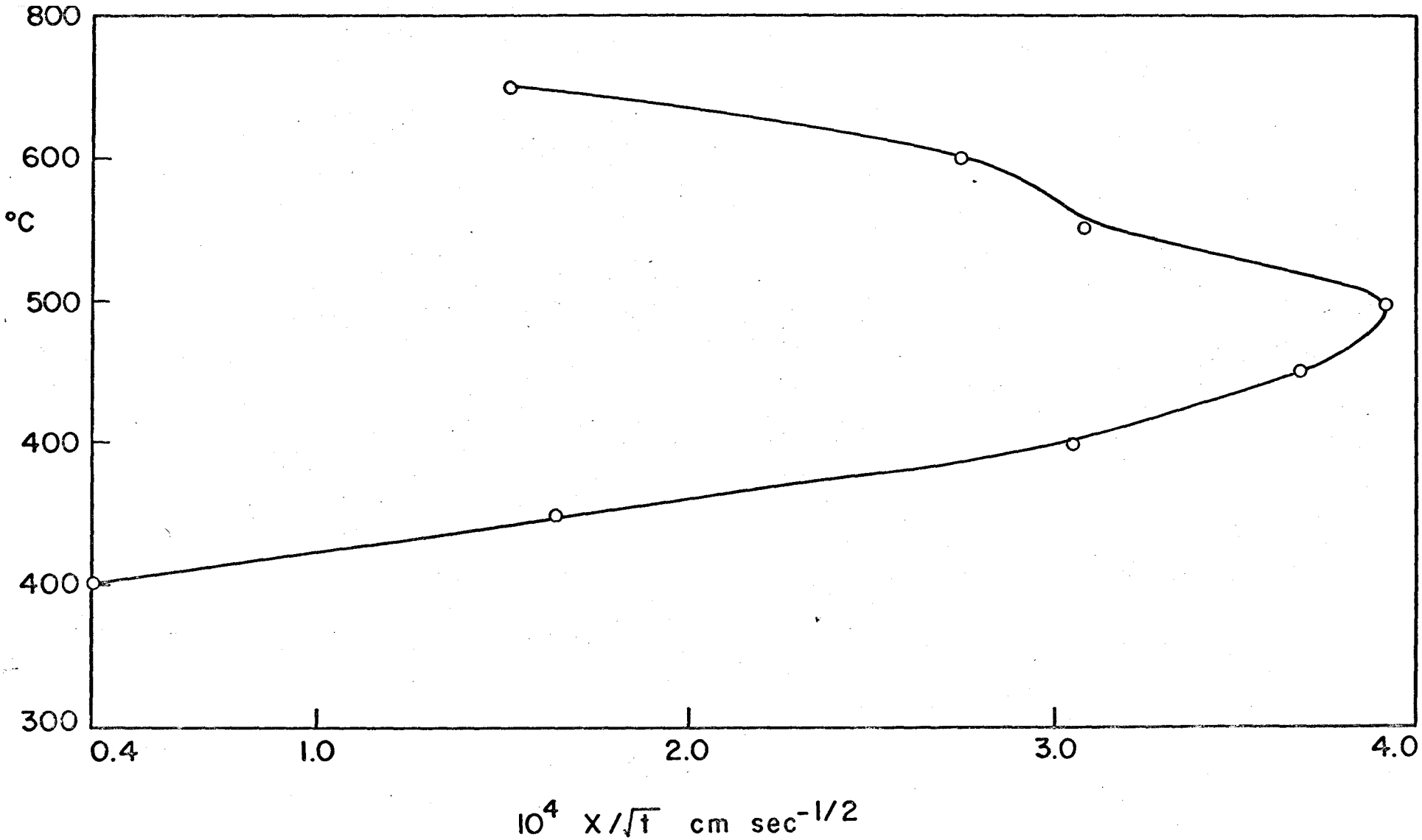

Fig. 22 Parabolic Growth Rate vs. Temperature for Widmanstatten α from β (60.4 wt % Cu brass)

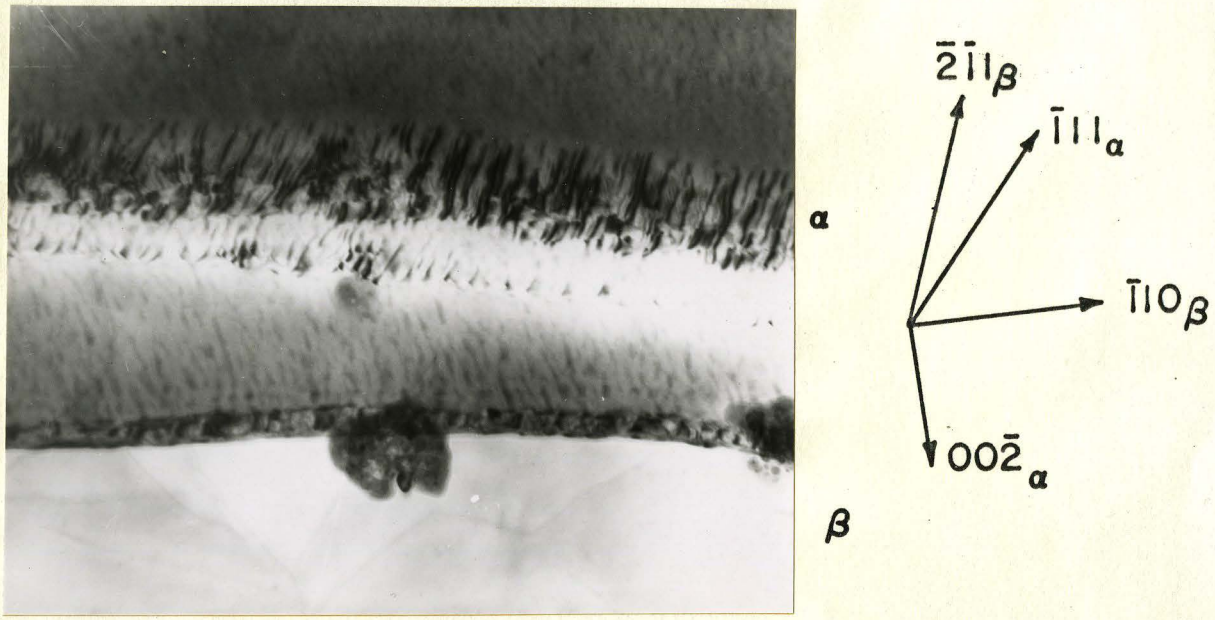

Fig. 23. Widmanstatten α-β interface showing α formed from tempering at 200°C for 1 hr. X 90,000

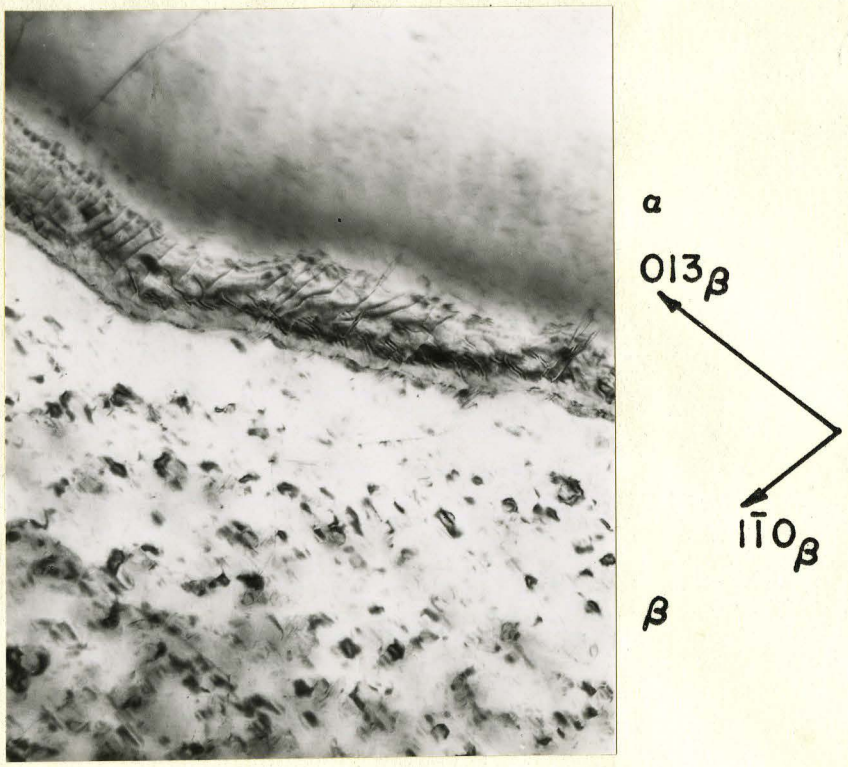

Fig. 24. α-β interface formed on tempering at 200°C for 1 hr. showing a high density of facets. Note precipitation in the β-phase. X 60,000

Fig. 25. α-β interface formed on tempering at 200°C for 1 hr. showing interface facets and dislocations X 120,000

Fig. 26. Optical micrograph of Widmanstatten precipitate formed on reacting the metastable β' phase at 500°C for 1 min. X 600

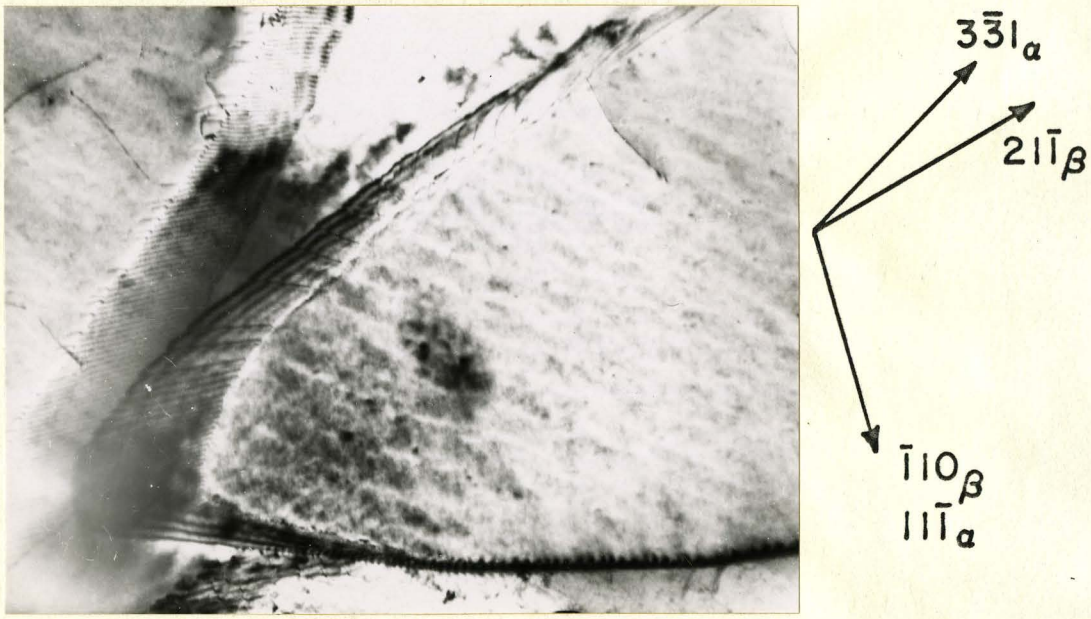

Fig. 27. Widmanstatten plate showing faceting and dot contrast in the α phase. X 60,000

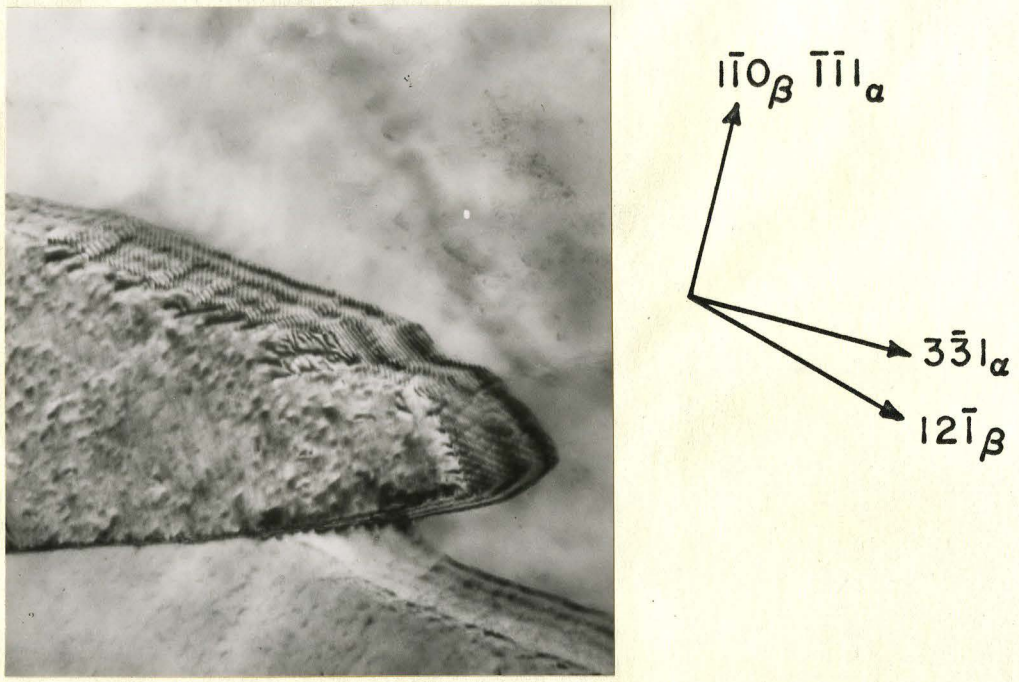

Fig. 28. Widmanstatten plate formed at 500°C, exhibiting facets and a moire effect. X 60,000

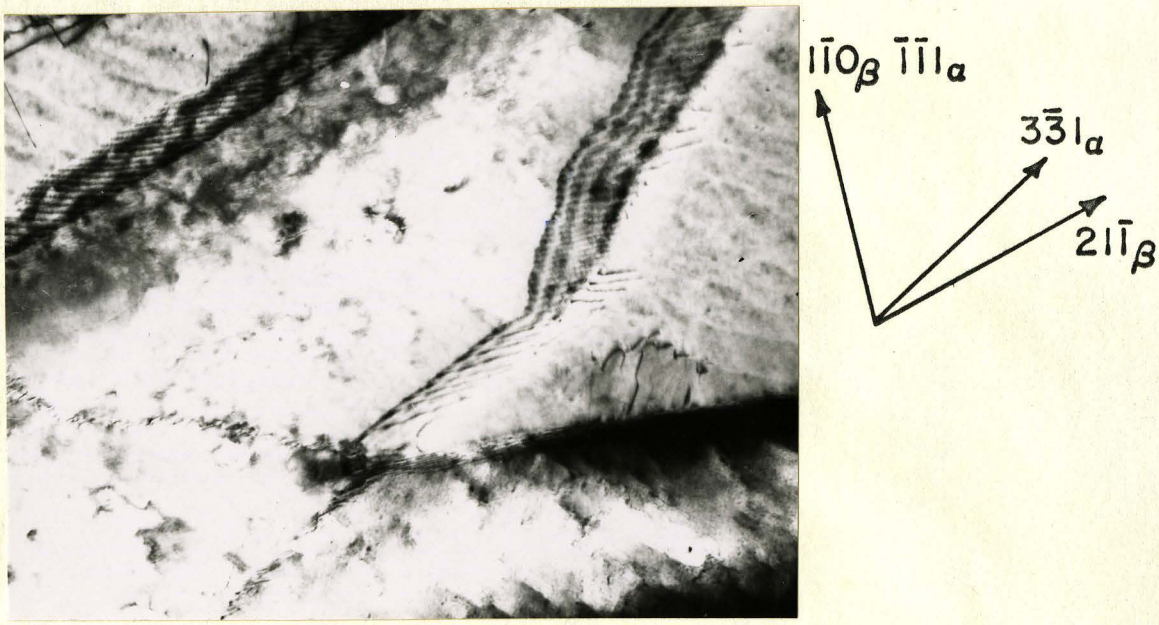

Fig. 29. Widmanstatten plate showing facets formed at 500°C. Note apparent subgrain formed by dislocations emenating from the tip of the plate. X 60,000

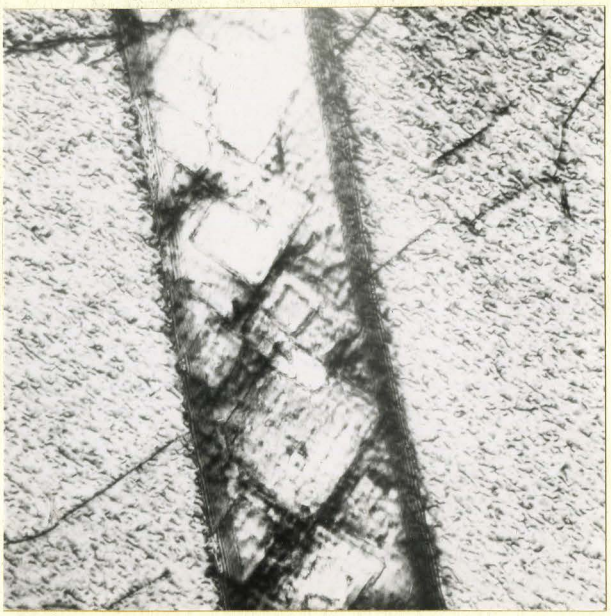

Fig. 30. Isothermally formed Widmanstatten plates tempered at 200°C for 1 hr. showing precipitation in retained β phase.
X 60,000

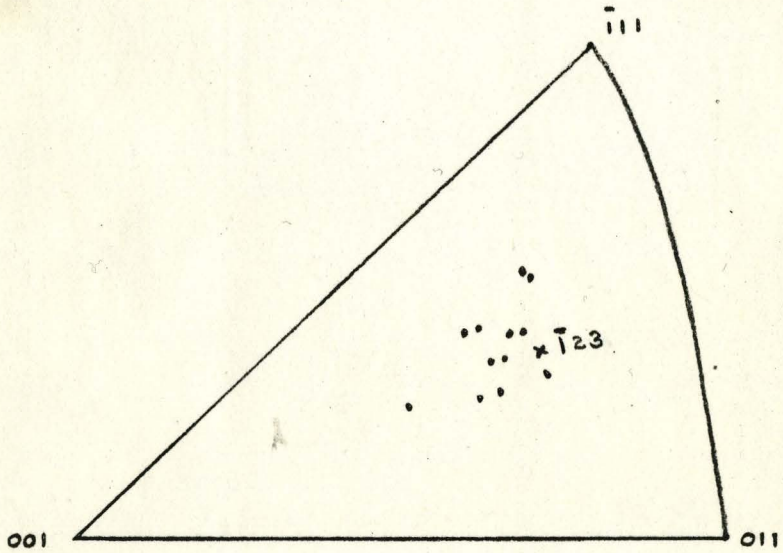

Fig. 31 Trace analysis of facets formed at 500°C and 200°C